Contrib Mineral Petrol (1988) 100:300–324

Contributions to Mineralogy and Petrology

The Miocene-Pliocene Macusani Volcanics, SE Peru

I. Mineralogy and magmatic evolution of a two-mica aluminosilicate-bearing ignimbrite suite

Michel Pichavant[1], Daniel J. Kontak[2]*, Jacinto Valencia Herrera[3] and Alan H. Clark[2]

[1] Centre de Recherches Pétrographiques et Géochimiques BP 20, F-54501 Vandoeuvre les Nancy, France
[2] Department of Geological Sciences, Queen's University Kingston, Ontario K7L 3N6, Canada
[3] Instituto Peruano de Energia Nuclear Av. Canada, 1470, Lima 13, Peru

Abstract. The Miocene-Pliocene Macusani volcanics, SE Peru, outcrop in three separate tectonic intermontane basins developed on a Paleozoic-Mesozoic volcano-sedimentary sequence. Several ignimbrite sheets are recognized and K – Ar dates record at least semi-continuous volcanic activity from 10 to 4 Ma in the Macusani field. The volcanics in the Macusani basin comprise crystal-rich (45% crystals) ash-flow tuffs and rare obsidians glasses, both with unusual mineralogy, similar to two-mica peraluminous leucogranites. The mineralogical assemblage (quartz, sanidine Or_{69-75}, plagioclase, biotite, muscovite and andalusite (both coexisting in the entire volcanic field), sillimanite, schörl-rich tourmaline, cordierite-type phases, hercynitic spinel, fluor-apatite, ilmenite, monazite, zircon, niobian-rutile) is essentially constant throughout the entire Macusani field. Two distinct generations of plagioclase are recognized, *viz.* group I (An_{10-20}) and group II (An_{30-45}). Sillimanite forms abundant inclusions in nearly all phases and is earlier than andalusite which occurs as isolated phenocrysts. Biotite (Al-, Ti-, Fe- and F-rich) shows pronounced deficiencies in octahedral cations. Muscovite is also F-rich and displays limited biotitic and celadonitic substitutions. There is no systematic variation in mineral chemistry with stratigraphic position. The mineralogical data provide a basis for distinction between an early magmatic and a main magmatic stage. The early stage corresponds to the magmatic evolution at or near the source region and includes both restites and early phenocrysts. Some biotites (with textures of disequilibrium melting to Fe – Zn spinel), part of the sillimanite, apatite and monazite, possibly some tourmaline and cordierite-type phases are restites. However, the restite content of the magma was low (5 vol. % maximum). The group II plagioclase are interpreted as early phenocrysts. During this stage, temperatures were as high as 800° C, pressure was no more than 5–7.5 kbar, fO_2 was intermediate between WM and QFM and a_{H_2O} was low. The biotite melting textures and the coexistence of restites and early phenocrysts imply fast heating rates in the source region. The transition between the early and the main magmatic stage was abrupt (andalusite crystallization in place of sillimanite, group I vs. group II plagioclases) and suggests rapid ascent of the magma from its source region. During the main crystallization stage, temperature was 650° C or lower at a pressure of 1.5–2 kbar. a_{H_2O} (calculated from equilibrium between muscovite, quartz, sanidine and andalusite) are around 1, suggesting conditions close to H_2O-saturation. f_{HF} is around 1 bar but the f_{H_2O}/f_{HF} ratios are significantly different between samples. f_{H_2} ranges between 138 and 225 bar. This study shows that felsic, strongly peraluminous, leucogranitic magmas having andalusite and muscovite phenocrysts may be generated under H_2O-undersaturated conditions.

Introduction

Peraluminous volcanic rocks provide direct information on crustal melting processes. Here, we document critical features of the Miocene-Pliocene peraluminous volcanics from the Macusani area, SE Peru. Compared to previously described peraluminous volcanic suites (e.g., Zeck 1970; Wyborn et al. 1981; Clemens and Wall 1984; Munksgaard 1984), the Macusani volcanics are unusual and may represent volcanic equivalents of two-mica peraluminous leucogranites. As such, they provide a rare opportunity to study the magmatic evolution of felsic, strongly peraluminous magmas. Francis (1959) and Barnes et al. (1970) provided the first descriptions of the geology of these volcanics. However their critical importance was only recently recognized through the preliminary work of Kontak et al. (1984a), Noble et al. (1984) and Valencia Herrera et al. (1984). As part of a continuing project on the Macusani volcanics, we describe the regional and local geological setting and report new K – Ar ages. More specifically, we focus on the petrography and mineralogy of the rocks. The Macusani volcanics provide decisive evidence on the significance of mineral phases in felsic peraluminous magmas and on their composition (e.g., Clarke 1981; Chappell et al. 1987). The P – T – a_{H_2O} – fO_2 conditions during the magmatic evolution can also be determined. The geochemical features of the Macusani volcanics are presented in Part II (Pichavant et al. 1988), together with a model for magma generation.

Regional and local geological setting

The volcanics of the Macusani formation (or Macusani volcanics) are located in the *Cordillera Oriental* region (s.l.) of the Central

* *Present address:* Nova Scotia Department of Mines and Energy PO Box 1087, Halifax, Nova Scotia A1B 2X1, Canada

CRPG Contribution n° 769

Offprint requests to: M. Pichavant

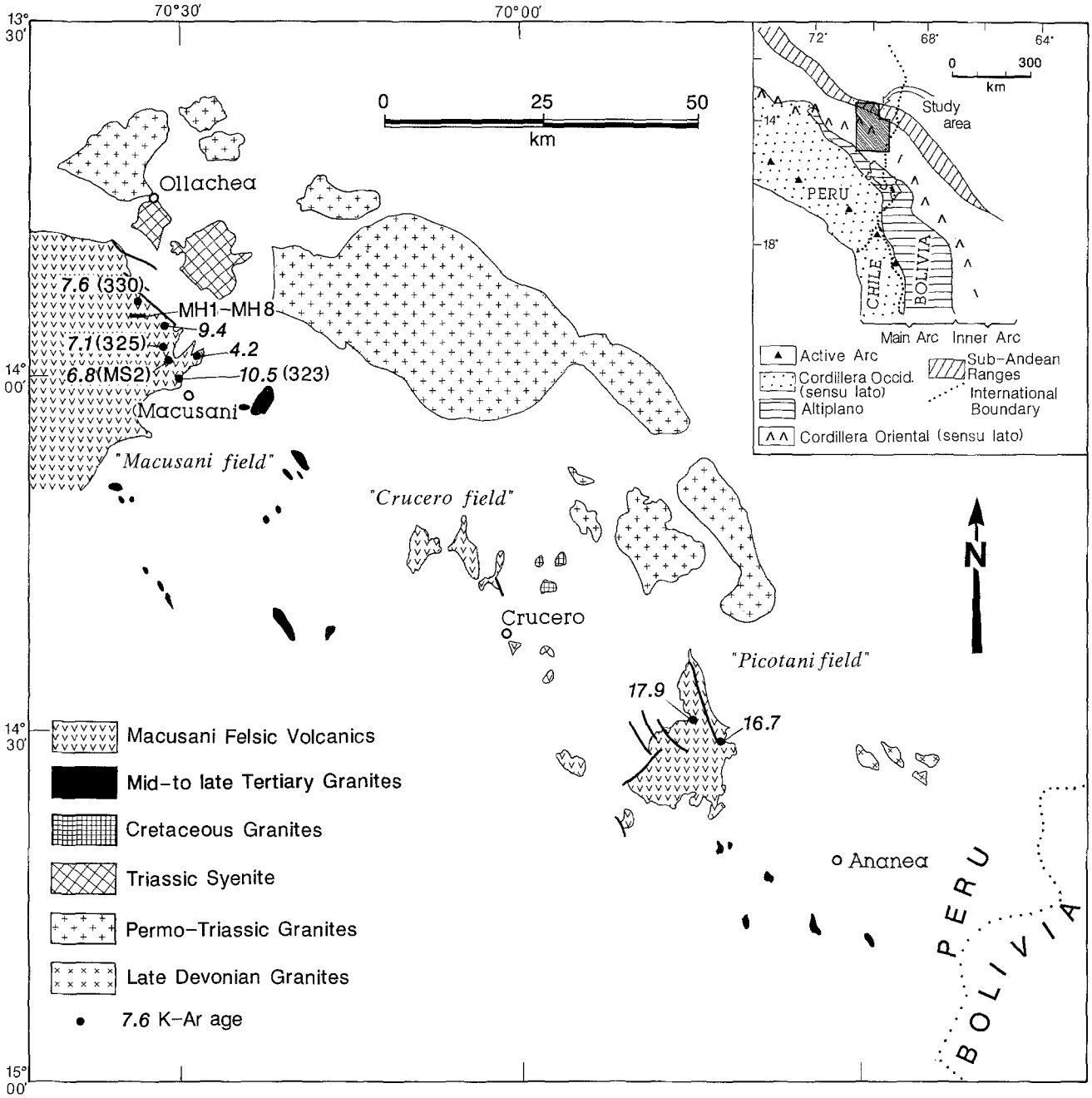

Fig. 1. Location of the study area in the Cordillera Oriental region of SE Peru (*inset*). K – Ar mica dates are given. The 4.2 Ma age is from Barnes et al. (1970) and the 9.4 Ma age from Noble et al. (1984). Some of the sample locations of the Macusani volcanics are indicated (Huiquiza section, samples MH1 to MH8, see also Fig. 2; samples 323, 325, 330 and MS 2, Kontak (1985), see also Table 1 and text). The distribution of the igneous rocks is taken from Laubacher's (1978) regional map

Andes (Fig. 1), forming part of the Inner Arc magmatic domain (Clark et al. 1984). In contrast to the better-studied Main Arc system which is characterized by subduction-zone related, quasi-continuous magmatism and tectonism (e.g., James 1981; Kulm et al. 1981; Harmon and Barreiro 1984; Pitcher et al. 1985), the Inner Arc domain is characterized by its history of ensialic-type tectonism and episodic magmatism of dominantly crustal nature (Clark et al. 1984; Kontak et al. 1984b; Kontak 1985).

The geology of the *Cordillera Oriental* region of SE Peru has been described by Laubacher (1978); more recently Kontak (1985) has emphasized the magmatic, metamorphic, metallogenetic and geochronological evolution of the area. A cursory review of the geology is warranted, however, since we will refer to these rocks in our later discussion of the petrogenesis of the Macusani volcanics.

The area is underlain by 10–15 km of pelites and psammites of Ordovician to Devonian age, presumably deposited on an unexposed Precambrian basement (Lehmann 1978; Injoque et al. 1983). Following a period of regional deformation and localized plutonism (ca. 350 Ma, Fig. 1), an upper Paleozoic-Mesozoic succession of quartzites, shales, carbonates and molasse (red-beds, alkaline volcanics) was deposited. This was followed by emplacement of Permo-Triassic (ca. 235 Ma) granitoid batholiths along the length of the *Cordillera Oriental*, local syenitic plutonism in the Jurassic (ca. 185 Ma), minor granodioritic magmatism in the Cretaceous (80–70 Ma), and strongly peraluminous Tertiary magmatism in the

Table 1. Analytical data for conventional K – Ar dating of the Macusani volcanic rocks

Sample	Lat. S	Long. W	Mineral	% K	^{40}Ar(rad.) $cm^3/g \times 10^{-5}$ STP	^{40}Ar % atmos.	Apparent age $\pm 2\sigma$ (Ma)
437	14°27′30″	69°45′00″	muscovite	8.081	0.564	51.9	17.9±0.6
TsVm1	14°00′25″	69°41′35″	biotite	7.227	0.472	34.1	16.7±0.4
323	14°01′20″	70°27′00″	biotite	6.880	0.280	77.1	10.5±0.5
330	13°53′16″	70°32′43″	biotite	7.304	0.216	57.2	7.6±0.3
325	14°00′00″	70°28′30″	biotite	7.272	0.202	54.9	7.1.±0.7
MS 2	14°00′40″	70°27′43″	biotite	7.289	0.192	43.8	6.8±0.2

Analyses carried out at Geochronology Laboratory, Department of Geological Sciences, Queens' University, Kingston, Ontario (details of the technique in Kontak 1985) on mineral separates from ash-flow tuffs. Potassium analyses are averages of duplicate runs (estimated precision ±0.7% (2σ)). Ages were calculated using constants recommended by Steiger and Jäger (1977)

form of small granitic stocks (27–8 Ma, Clark et al. 1983; Kontak et al. 1987) plus felsic volcanics (the Macusani suite: 17–4 Ma). In terms of the volume of magma emplaced into the crust during these periods, we emphasize that the crustal component greatly exceeded the mantle component and that, in many instances, it has been shown that there is a very close temporal and spatial relationship between the two contributions (e.g., late Devonian, Permo-Triassic, Tertiary granites: Kontak 1985; Kontak et al. 1986).

The Macusani volcanics outcrop in three main separate places within the study area, the "Macusani", "Crucero" and "Picotani" fields (Fig. 1). They occupy tectonic intramontane basins oriented NW-SE (Fig. 1). The volcanics are well exposed in all three localities, but detailed mapping has not been completed. Hence, it is premature to discuss any large scale volcanological features (calderas, cf. Noble et al. 1984). As a result of the cursory nature of the mapping of these rocks, only an approximation of the areal extent and volume of magma erupted is attempted. For the Macusani field, the extent of this lithology indicated on Laubacher's (1978) regional map is ca. 1200 km^2, considerably less than the 2500 km^2 suggested by Noble et al. (1982, 1984). Recent mapping in the southwestern part of this field by Arenas (1982) reveals that much of the area consists of rocks belonging to the Tacaza Group (Newell 1949), including andesites, volcanic breccias and rhyolitic tuffs. Thus, the 500 km^2 areal extent for this field suggested by Valencia Herrera et al. (1984), while being conservative, is considered a closer approximation to the true value. In the same manner, it is difficult to estimate the volume of volcanic material because a three-dimensional picture is not available. However, our preliminary work indicates that the pre-eruption topography was quite irregular, with at least local canyon development in the Paleozoic-Mesozoic basement rocks. This can be observed, for example, along the Rio San Gaban at the northeastern extremity of the field. A conservative estimate for the volume of volcanic rocks preserved is 200–250 km^3 corresponding to a maximum thickness of 500 m. The Macusani field is separated from the Crucero and the Picotani fields by a prominent topographic high. Thus, it is likely that these represent separate fields, indicating at least two separate areas of magmatic activity. The Crucero and Picotani fields occupy a topographic low (the Crucero-Ananea depression, Laubacher 1978) and may represent the remnants of a once-continuous volcanic field. The estimated areal extent is 1500 km^2, with a volume of 300 km^3. Preliminary studies by one of us (AH Clark) indicate that the central area of the Picotani field is underlain by a group of subvolcanic granites (see also Clark et al. 1987). The small basaltic flows outcropping in the Picotani field represent one of the few exposures of basic rocks in this area of the *Cordillera Oriental*. These flows are located stratigraphically below the Macusani formation and there is no apparent relation between the two volcanic units.

The Macusani volcanics consist of numerous, easily recognizable ignimbrite sheets of variable thickness (10 m to in excess of 100 m). Although generally flat-lying, irregular dips are observed, reflecting the irregular topography and block faulting contemporaneous with volcanism. Individual units are locally separated by unconsolidated gravel beds of several meters thickness (see Fig. 2). The individual sheets are massive and homogeneous throughout, lacking any features suggestive of welding. In some areas, vertical "cooling" joints are developped.

K – Ar ages

Several new K – Ar mica (biotite and muscovite) ages have been obtained for the Macusani volcanics (Fig. 1 and Table 1). The oldest ages, 17.9±0.6 Ma and 16.7±0.4 Ma, were obtained for the volcanics of the Picotani field (samples 437 and TsVm1, Table 1) and the older of the two ages was for a sample collected at the lowest exposed horizon in the unit. The two ages are significantly different at the 95% confidence level and indicate that volcanic activity spanned a minimum of ca. 1 Ma in this region.

The remaining ages were obtained for samples from the Macusani field and, in Fig. 1, are compared to the previous age determinations of Barnes et al. (1970: 4.2±1.0 Ma for an ash-flow tuff, 4.3±1.5 Ma for an obsidian glass or macusanite. Both ages are recalculated to new constants; see also Pichavant et al. 1987a) and Noble et al. (1984: 9.4±0.3). Sample 330, dated at 7.6±0.3 Ma, was collected from the apparent base of the Macusani field along the Rio San Gaban where the volcanics unconformably overlie Permian sediments and volcanics of the Mitu Group (Newell et al. 1953). In contrast, sample 323 was collected from the apparent top of the section traversed and it gave an age of 10.5±0.5 Ma. Thus, the results of the K – Ar dating indicate that the internal stratigraphic relationships of the Macusani field are probably complex. The most important result of this dating, however, is the documentation of continuous, or at least semi-continuous, eruption of silicic magma over a period of ca. 6 Ma.

Sample location and field description of the volcanics

In this paper, all samples are from the Macusani field except 437 and TsVm1 used for dating the Picotani field. Most samples come from the eastern part of the field (Fig. 1). Samples of ash-flow tuff used for dating and geochemistry (Pichavant et al. 1988) include MS2 and 323 to 330, collected along an oblique section from the apparent top to base (Fig. 1). For the detailed petrographic and mineralogical studies, the samples are mostly from the Huiquiza section (Valencia Herrera et al. 1984; Figs. 1 and 2, samples MH1 to MH8), but additional samples (about 60) from various parts of the field were studied. In addition, MA29 (Chilcuno Chico area), CEA1, CHA2, CHA13 (Chapi area, CEA1 provided by COGEMA), VB3 (provided by V E Barnes, Austin) and JV1, JV2 (obsidian glasses from the Chilcuno Chico area, Pichavant et al. 1987a and references therein) were retained for detailed mineralogical studies.

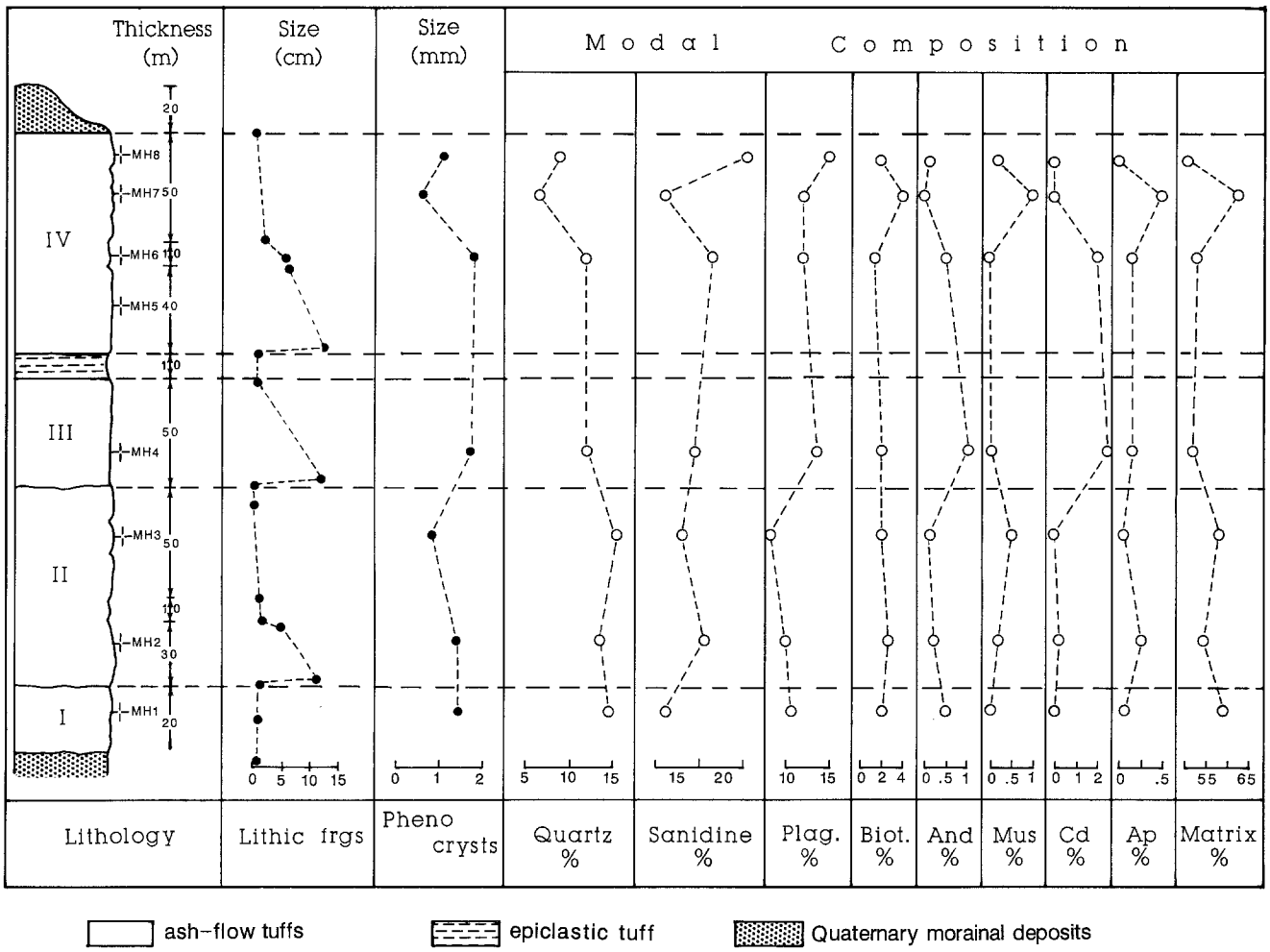

Fig. 2. Stratigraphic position of samples, petrography, and whole-rock modal composition (vol.%) of ash-flow tuffs along the Huiquiza section. The numbers I to IV refer to individual ash-flow sheets. *Plag*: plagioclase; *Biot*: biotite; *And*: andalusite; *Mus*: muscovite; *Cd*: cordierite-type phases (see text); *Ap*: apatite

The Huiquiza section (Fig. 2) offers continuous outcrop in the stratigraphically-lower units of the preserved volcanic sequence and four separate flow units have been distinguished. Some contacts between units are underlain by erosional horizons, and an epiclastic tuff separates units III and IV. The base of each flow unit is marked by an increase in the size of the lithic fragments (very low-grade or non-metamorphic inclusions of pelites, limestones and quartzites from the country rocks). Field studies in various other parts of the volcanic field revealed the presence of additional types of inclusions, i.e., pumice fragments and centimetric inclusions of rhyolite (with a mineralogy similar to that of the tuffs). Inclusions of foreign volcanic material have not been observed.

The volcanics are very homogeneous and consist of grey, poorly consolidated ash-flow tuffs. The tuffs are crystal-rich (average 45 vol. % crystals, 1500 to 2000 points counted per thin section, Fig. 2). In contrast, the highly vesicular pumice fragments carry a significantly lower percentage of crystals (around 20 vol. %). The mineralogical composition does not change significantly throughout the entire volcanic field. Across the Huiquiza section, the change in modal proportions between samples is usually irregular, but one notes an overall tendency for quartz and matrix to decrease and for sanidine and plagioclase to increase from base to top (Fig. 2). Also the modal proportions of muscovite and andalusite vary antipathetically throughout the entire section (Fig. 2). A similar relationship between biotite and cordierite-type phases is observed in the Chapi area.

Mineralogy

Techniques

A total of about 80 thin sections have been examined and about 20 studied in detail by various techniques including U-stage, autoradiography, scanning electron microscopy and electron microprobe. Mineral phases were analysed using the Camebax electron microprobe at the Nancy I University. For most phases and elements, the analytical conditions were as follows: counting time on peak: 6 s, sample current: 6–8 nA, accelerating voltage: 15 kV, various silicate crystals as standards and ZAF correction procedures. Ilmenites and niobian rutiles were analysed with a longer counting time (20 s on peak) and acceleration voltage (20 kV). For zircons and monazites we counted for 15 s on peak. For hercynitic spinels, the PAP correction program (Pouchou and Pichoir 1984) was used instead of the ZAF. This new correction program gives better results for phases such as spinels that carry elements with greatly different Z and absorption coefficients (e.g., Fe and Al), allowing a better evaluation of the (Fe^{3+}/Fe^{2+}) ratio in the spinel. Fluorine in micas and tourmalines was analysed separately under higher counting time (10 s on peak) and sample current (40 nA). To avoid complex ZAF correction procedures for light elements such as F, the raw counts were averaged (usually from between 5 to 10 spots), then plotted against an internal calibration curve constructed from two standards (a Macusani glass and a fluorapa-

Table 2. Systematic textures in the Macusani ash-flow tuffs

Sillimanite inclusions in major phases, including andalusite; zonal disposition of sillimanite inclusions in quartz, sanidine and plagioclase (Fig. 4a, c, d)
Zonal arrangement of zircon inclusions in apatite (Fig. 8a)
Mantling of plagioclase by sanidine (Fig. 4d)
Small glomerocrysts (<1 mm) with biotite, muscovite, andalusite and sanidine

Table 3. Textural relations among mineral phases

	hosts									
	Qz	Sa	Plag	Biot[b]	Mu	And	Sill	Cd	To	Ap
inclusions[a]										
Qz		+	+		+					
Sa	+		+		+					
Plag	+	+								
Biot	+	+[c]	+[c]		+	+		+		
Mu	+	+								
And		+	+							
Sill	+	+	+	+	+	+		+	+	+
Cd		+				+				
To		+	+	+?	+			+?		
Ap				+	+	+				

[a] Accessory minerals (ilmenite, monazite, zircon) not tabulated
[b] Spinels, sillimanite, andalusite, cordierite and plagioclase also found in sieve-textured biotites
[c] Includes biotite associated with spinels

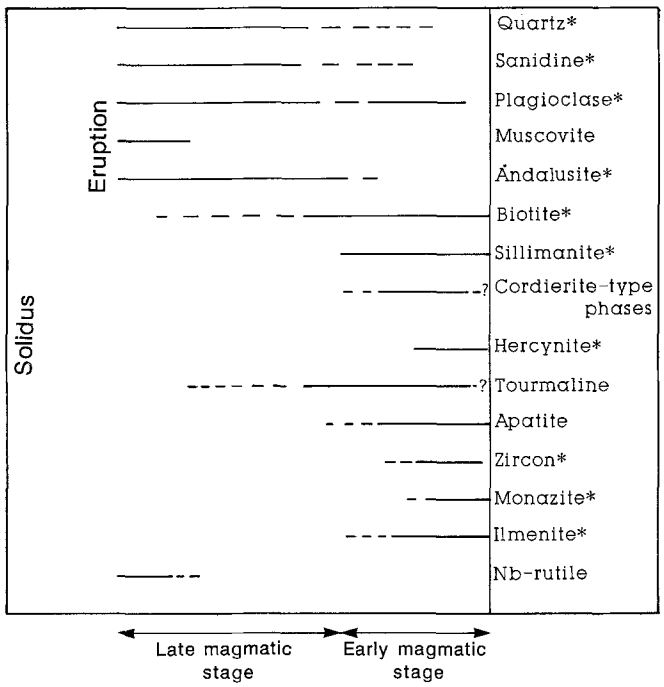

Fig. 3. Crystallization sequence for the Macusani volcanics. Mineral phases labelled with asterisks are also present in the Macusani obsidian glasses (Pichavant et al. 1987a). Virgilite (present in the Macusani glasses, French et al. 1978) has not been found in the tuffs

tite) and the concentrations thus determined. Ba in sanidine and Zn in biotite (Montel et al. 1986b) were also analyzed separately.

Mineral phases and mutual relations

There is no significant compaction and welding of the volcanics. The matrix is devitrified and heavily altered to a mixture of clay minerals (kaolinite and montmorillonite). In contrast, most crystals are unaltered. They are commonly broken, but with evidence of little relative transport of the fragments.

Summaries of the textural relations are presented in Tables 2 and 3, while a list of mineral phases together with their crystallization order is given in Fig. 3. The study of secondary mineral phases (i.e., vapour-deposited or hydrothermal phases) is beyond the scope of this study. Tourmaline, spinel, cordierite-type phases (Kontak et al. 1984a; Valencia Herrera et al. 1984), monazite and niobian rutile were not reported by Noble et al. (1984 and references therein). Mullite (Francis 1959) was not found. Most of the phases encountered in the ash-flow tuffs are also present in the Macusani obsidian glasses (Fig. 3). However, muscovite, tourmaline, apatite, cordierite-type phases and niobian rutile were not found in the obsidian glasses, while virgilite (French et al. 1978) was not found in the tuffs. French and Meyer (1970) report gahnite and chromite from an HF residue of Macusani obsidian glasses, in agreement with the presence of Zn-rich spinels in the tuffs (see below). The presence of chromite is puzzling, given the very low Cr in the volcanics (Pichavant et al. 1987a, 1988). Linck (1926) reported the presence of several additional mineral phases in the obsidian glasses.

Quartz forms euhedral-subhedral crystals of the high temperature habit (β-quartz), frequently embayed and containing partially crystallized melt inclusions or zonally distributed sillimanite needles (identified both optically and by electron microprobe). The bulk of the quartz appears to be relatively late (Fig. 3).

Sanidine is subhedral-euhedral, it has an average 2V of 30° and commonly mantles plagioclase (Fig. 4d). This feldspar contains zonally disposed sillimanite inclusions (Fig. 4a), hosts most of the other major phases as inclusions and appears late in the crystallization sequence (Fig. 3).

The various *plagioclase* textures have been divided into two groups (Fig. 4). Group I comprises isolated crystals (Fig. 4b, c), inclusions in sanidine or quartz, rare mantles around sanidine, small plagioclases associated with sieve-textured biotites and rims around earlier plagioclase cores. These plagioclases are commonly subhedral-euhedral; they display oscillatory zoning and several episodes of growth (Fig. 4b, c). Biotite and sillimanite (Fig. 4c) are the main inclusions (see also Table 3). Textural relations with quartz and sanidine suggest cotectic crystallization during the main magmatic stage (Fig. 3). The group II plagioclases are restricted to cores in group I plagioclases. These cores are rather rare (a few crystals per thin section) and they are absent from plagioclase crystals in the glasses. They are generally small (a few hundreds μm) and the boundary between core and rim is sharp (Fig. 4d, e). Note that the sillimanite inclusion ring is always found in the rim, i.e., is external to the core-rim boundary (Fig. 4d). These cores,

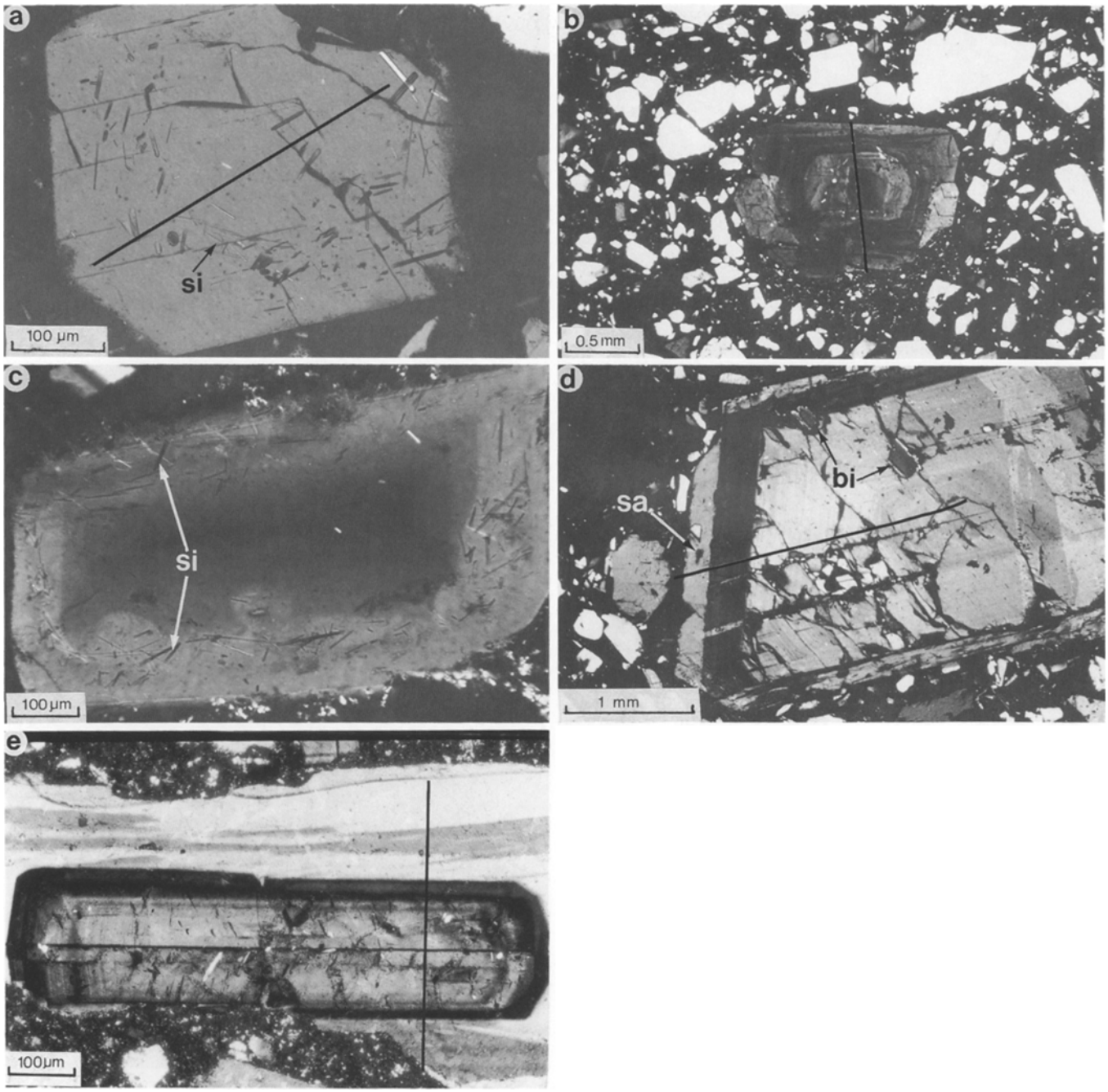

Fig. 4a–e. Feldspars in the Macusani ash-flow tuffs. **a** isolated sanidine (Table 4, n° 1, 2) with zonally disposed sillimanite (*si*) inclusions, sample MH3; **b** isolated group I plagioclase with oscillatory zoning and several stages of growth (Table 4, n° 6; Fig. 10a), sample MH7; **c** strongly zoned isolated group I plagioclase with zonally disposed sillimanite (*si*) inclusions, sample MH6. Core: An_{25-30}, rim An_{14}. Note the absence of boundary between core and rim and the external position of the sillimanite inclusion ring; **d** group II plagioclase core (Table 4, n° 8; Fig. 10c) with a group I plagioclase rim (Table 4, n° 7; Fig. 10c) mantled by sanidine (*sa*) (external rim), sample CHA2. Note the sharp optical boundary between core and rim (compare with **c**). The inclusions of biotite (*bi*) (Table 5, n° 6) are associated with spinels (not visible). Also present, but not visible, is a sillimanite inclusion ring, similar to **c** in the albitic rim. **e** group II plagioclase core (Table 4, n° 9; Fig. 10b) with a group I plagioclase rim (Fig. 10b), sample MH3. In **a, b, d** and **e**, the *lines* are microprobe traverses (Fig. 10). Crossed Nicols for all microphotographs

with delicate oscillatory zoning and common twinning (Fig. 4d, e), are texturally early (Fig. 3).

Biotite appears either as small euhedral isolated crystals (Fig. 5a), as inclusions in muscovite, or more rarely, as crystals growing on feldspars (texturally the latest biotite observed in the tuffs). Biotite forms small (< 1 mm) glomeroclasts with muscovite, andalusite and sanidine. Another textural type is defined by larger (up to 5 mm), sieve-textured biotites (Fig. 5b). These occur sporadically but throughout the entire volcanic field. One of their characteristic features is the presence of *spinel* (Fig. 5b, c) in the sieve-textured zones. The occurrence of spinel in the ash-

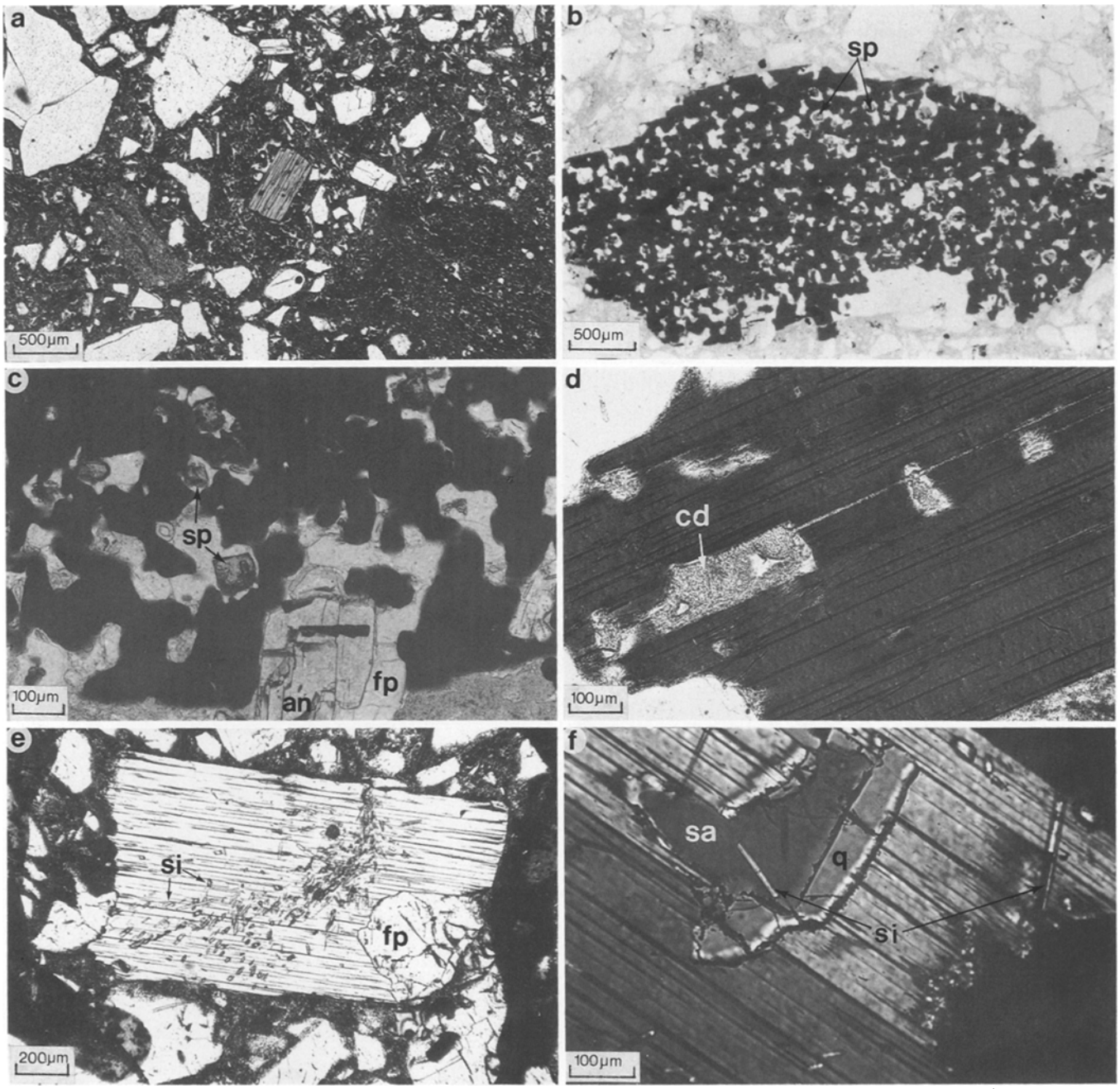

Fig. 5a–f. Micas in the Macusani ash-flow tuffs. **a** isolated biotite (Table 5, n° 1), sample MH1; **b** coarse sieve-textured biotite associated with spinels (*sp*) (Table 5, no° 5 and Table 8, n° 9–11), sample CEA1. Note the large number of spinel crystals; **c** enlarged view of **b** showing the sieve-textured zones with spinels (*sp*), feldspars (*fp*), rimmed by andalusite (*an*) containing biotite inclusions; **d** large sieve-textured biotite associated with altered cordierite-type phases (*cd*), sample CHA13; **e** large isolated muscovite (Table 5, n° 14) with coarse sillimanite (*si*) inclusions (Table 7, n° 13) and feldspar (*fp*), sample MH8; **f** muscovite hosting a quartz (*q*)-sanidine (*sa*) aggregate, sample MH7. Note the sillimanite inclusions (*si*) present in the muscovite as well as in the sanidine. Plane-polarized light for all microphotographs except **f** under crossed Nicols

flow tuffs is restricted to this texture. Cordierite-type phases (Fig. 5d) may sometimes replace spinel in the sieve-textured zones. Fragments of disrupted sieve-textured biotites with spinels occur in plagioclase (Fig. 4d) and sanidine, demonstrating that such biotites are early. Indeed, most textures suggest that biotite is an early phase (Fig. 3).

Muscovite forms euhedral crystals of variable size (up to 1 mm), and commonly contains inclusions of biotite (with sharp optical and chemical boundaries between the two phases), sillimanite and, less commonly, quartz and sanidine (Figs. 5e, f; 6e). Muscovite and andalusite coexist in most thin sections, although they were never observed in mutual contact. Muscovite is one of the latest major phases in the crystallization sequence (Fig. 3). The latest muscovites are found as mantles on sanidine.

Andalusite appears mostly as isolated euhedral-subhedral crystals (Fig. 6a) with a colourless-to-pink pleochroism, similar to that of andalusites from peraluminous leucogran-

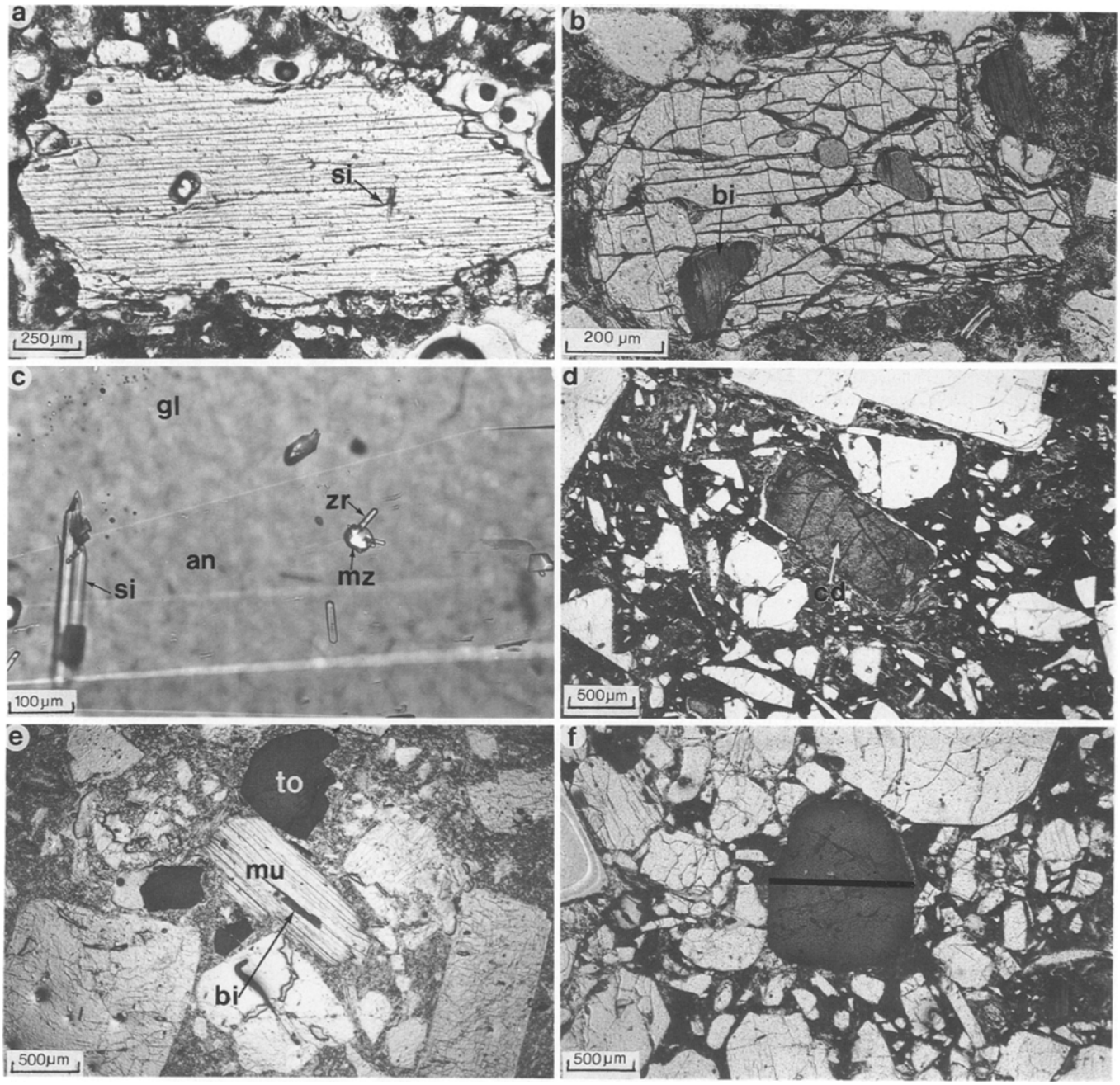

Fig. 6a–f. Al-silicates, tourmalines and cordierite-type phases in the Macusani ash-flow tuffs and obsidian glasses. **a** isolated andalusite (Table 7, n° 9–10) with a few sillimanite (*si*) inclusions, sample MH4; **b** andalusite with biotite (*bi*) inclusions (Table 5, n° 7), sample MH4; **c** andalusite (*an*) in a Macusani obsidian glass (*gl*) with inclusions of sillimanite (*si*), zircon (*zr*) and monazite (*mz*), sample JV2, compare with Linck (1926); **d** altered cordierite-type phase, sample CHA13; **e** isolated tourmaline crystals (*to*), sample MA29. Note the weak optical zonation in the tourmalines and the muscovite (*mu*) with a biotite inclusion (*bi*); **f** isolated tourmaline (Table 7, n° 4–5; Fig. 13) with sillimanite and zircon inclusions, sample CEA1. The *line* is the microprobe traverse (Fig. 13). Plane-polarized light for all microphotographs

ites and pegmatites (Clarke et al. 1976; Pichavant and Manning 1984). Andalusite commonly contains inclusions of sillimanite, apatite, ilmenite, zircon and monazite. It crystallizes later than biotite as shown by andalusites containing biotite inclusions (Fig. 6b) or growing around sieve-textured biotite (Fig. 5c). Conversely, andalusite is commonly included in sanidine and definitely earlier than muscovite. It is a characteristic mineral of the obsidian glasses (Fig. 6c, Pichavant et al. 1987a and references therein). In contrast, *sillimanite* is rarely found in isolation (Fig. 6c). It is an ubiquitous inclusion in most phases, occurring mostly as elongated needles, often zonally distributed and outlining the growth faces of the host crystal (Table 2 and Figs. 4a, c; 5e; 6f). However, coarse, prismatic, sillimanite inclusions may also be found. These inclusions are randomly distributed in crystals and they may form accumulations, particularly in feldspars, muscovite (Fig. 5e) and andalusite. From textural relations, summarized in Table 3, there is no evi-

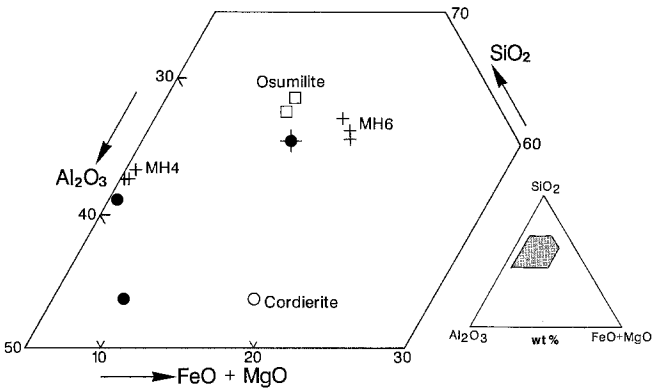

Fig. 7. $Al_2O_3 - SiO_2 - (FeO + MgO)$ plot showing the contrasted compositions of the cordierite-type phases in samples MH4 and MH6. (●): pinite (Marchand et al. 1982; Haslam 1983). (□): osumilite (Schreyer et al. 1983). (◆): beidellite-nontronite (Schenk and Ambruster 1985). (○): cordierite (Montel et al. 1986a)

dence for contemporaneous crystallization of the two aluminium silicates. Sillimanite is definitely earlier than andalusite. Sillimanite is the aluminium silicate typical of the early magmatic stage whereas andalusite is associated with the main magmatic stage (Fig. 3). In addition, there is no obvious indication of reaction between the two Al-silicates.

Tourmaline occurs mostly as small, subhedral, isolated crystals (Fig. 6e). However, large euhedral crystals are also present (Fig. 6f). This phase contains inclusions of sillimanite and accessories (Fig. 6e, f). Optical zonation is either absent or weak, from pale olive-green cores to dark olive-green rims. Tourmaline is generally early (Fig. 3) and inclusions of it can be found in feldspars and other major phases (Table 3). There are only few examples of texturally-late tourmalines (tourmaline overgrowths on earlier nuclei or small crystals growing on feldspars).

Cordierite-type phases occur as euhedral-subhedral remnants pseudomorphosed by phyllosilicates (Fig. 6d). They may be found either in isolation, as inclusions in feldspars, or, more rarely, in the sieve-textured biotites (Fig. 5d). Some contain small oriented biotite inclusions. Microprobe analyses (Table 7) yield two compositionally distinct groups (Fig. 7). One group (sample MH4) has compositions close to typical pinites (Marchand et al. 1982, Fig. 7). These are interpreted as alteration products of earlier *cordierites*. The other group (sample MH6) plots outside of the compositional field typical of pinite and instead falls close to *osumilite* and to beidellite-nontronite (a rare type of alteration product of cordierite, Fig. 7). These compositions may be interpreted either as alteration products of earlier osumilite or as peculiar alteration products of earlier cordierite. In any case, all the cordierite-type phases are early (Fig. 3).

Apatite occurs as coarse (up to 1 mm) euhedral-subhedral isolated crystals (Fig. 8a) and hosts numerous inclusions of various types, including fluid and possibly melt inclusions, monazite, zircon, ilmenite and sillimanite (Fig. 8b). A zonal disposition of the sillimanite and zircon inclusions is locally evident (Fig. 8a). Textures indicate that apatite is early (Fig. 3).

Ilmenite is the only opaque phase found in the Macusani tuffs and glasses. Noble et al. (1984) briefly mention the finding of a low-Ti opaque phase, presumably magnetite. Ilmenite is an early phase and is mainly found as inclusions in the other minerals, although small isolated ilmenites also occur.

Some thin sections contain a few small, dark-brown, isolated crystals of *niobian rutile* hosting monazite and zircon inclusions. This mineral is found only in samples containing dark-brown, altered biotites and we tentatively relate the crystallization of niobian rutile to a late stage of biotite alteration (see Table 6 for data on Nb in biotite), perhaps during emplacement of the ignimbrite sheets.

Zircon and *monazite* (initially distinguished from zircon by autoradiographies) occur in intimate spatial association. Both are systematically included in apatite crystals (Fig. 8b), and appear as inclusions in biotite, andalusite (Fig. 6c) and less frequently in quartz and feldspar. These two phases differ markedly in shape and size. Zircons are small (<20 μm) elongated crystals with well-developed prism faces and are similar in typology to zircons from two-mica granites (J P Pupin, pers. comm., 1986) whereas monazites form coarser (30–50 μm) crystals. Rarely zircon shows textural evidence of earlier cores (Fig. 8b). Both phases are early.

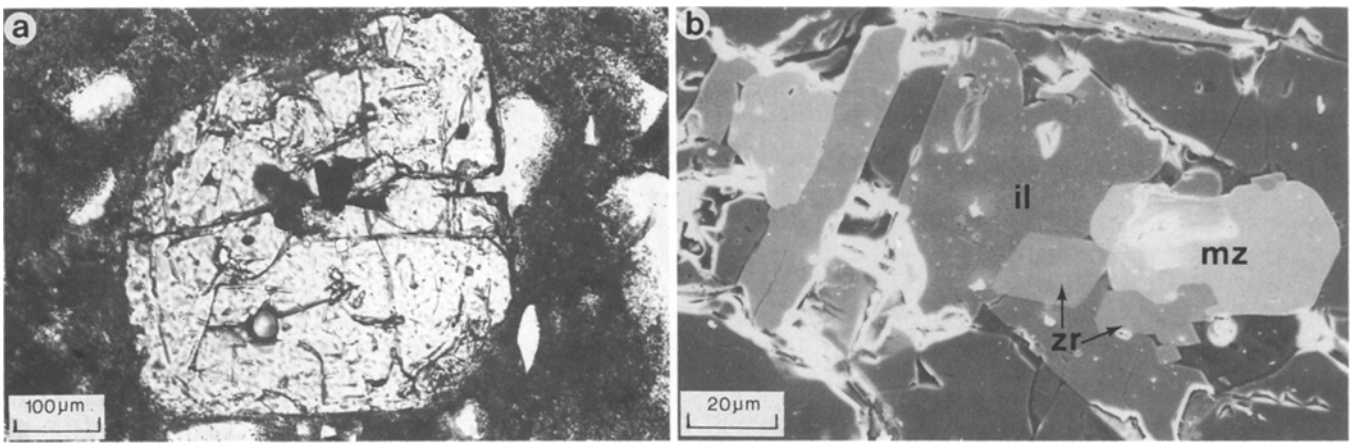

Fig. 8. a isolated apatite (Table 9, n°. 1–2) with zonally disposed sillimanite and zircon inclusions in the Macusani ash-flow tuffs, sample MH2, plane-polarized light; **b** enlarged SEM image of (a) showing ilmenite (*il*) (Table 8, n° 1), monazite (*mz*) and zircon (*zr*) inclusions. Note the cored zircon

Table 4. Representative electron microprobe analyses of sanidine and plagioclase

	MH3		JV2	MH3	MH6	MH7	CHA 2		MH3	JV2
	1	2	3	4	5	6	7	8	9	10
SiO_2	65.24	65.18	64.75	65.32	61.38	64.23	64.79	59.19	57.28	64.20
Al_2O_3	18.84	18.91	18.96	21.62	23.52	23.34	21.93	25.99	26.41	22.14
CaO	0.00	0.00	0.00	2.15	4.17	3.93	3.14	8.08	8.31	2.30
Na_2O	3.31	3.33	3.55	9.71	8.69	9.07	9.22	6.73	6.15	9.38
K_2O	11.76	11.71	11.33	0.85	0.68	0.57	0.87	0.41	0.27	0.79
BaO	0.01	0.12	n.d.	n.d.	n.d.	n.d.	n.d.	n.d.	n.d.	n.d.
Total	99.16	99.25	98.59	99.65	98.44	101.14	99.95	100.40	98.42	98.81
Si	5.98	5.98	5.97	5.77	5.53	5.61	5.72	5.27	5.20	5.72
Al	2.04	2.04	2.06	2.25	2.50	2.40	2.28	2.73	2.83	2.33
Ca	0.00	0.00	0.00	0.20	0.40	0.37	0.30	0.78	0.81	0.22
Na	0.59	0.59	0.63	1.66	1.52	1.54	1.58	1.16	1.08	1.62
K	1.38	1.37	1.33	0.10	0.08	0.06	0.10	0.05	0.03	0.09
Or	71	70	68	5	4	3	5	3	2	5
Ab	29	30	32	85	76	78	80	58	56	84
An	0	0	0	10	20	19	15	39	42	11

Structural formulae calculated on the basis of 16 O. End-members in mole %. *1*: isolated sanidine, rim (Fig. 4a); *2*: isolated sanidine, core (Fig. 4a); *3*: sanidine, Macusani glass; *4*: plagioclase inclusion in sanidine; *5*: plagioclase in sieve-textured biotite; *6*: isolated plagioclase (Fig. 4b); *7*: plagioclase rim (Fig. 4d); *8*: same crystal, plagioclase nucleus (Figs. 4d and 10c); *9*: plagioclase nucleus (Figs. 4e and 10b); *10*: plagioclase, Macusani glass. n.d. = not determined

Mineral chemistry

Sanidine major element compositions are given in Table 4 and the entire data set is plotted on Fig. 9. The composition of sanidine ranges from $Or_{69}Ab_{31}$ to $Or_{75}Ab_{25}$ (Fig. 9); Ca is always very low (less than 1 wt % An). Sanidine crystals in the obsidian glasses have identical compositions (Table 4). The composition of sanidine is nearly constant from one crystal to another in a given sample and from one sample to another in the stratigraphic sequence (Fig. 15). In an attempt to detect systematic chemical trends, sanidine was scanned for major elements and for Ba. For the crystal of Fig. 4a, there is no detectable change in major element composition between core (i.e., inside the sillimanite inclusion ring) and rim. In contrast, the Ba scan reveals strong zoning (rim below 300 ppm BaO, core average 1000 ppm, up to 2000 ppm BaO, Table 4). Thus, the sanidine records an abrupt depletion of Ba in the melt during crystallization (Mehnert and Büsh 1985).

Selected *plagioclase* compositions are given in Table 4 and the whole data set is plotted in Fig. 9. Most group I plagioclases cluster between $Ab_{85}An_{10}Or_5$ and $Ab_{76}An_{20}Or_4$ (Fig. 9). Plagioclases in the obsidian glasses (Table 4) are close to the most albitic compositions in group I. Rare, strongly zoned, group I plagioclases (Fig. 4c), some inclusions in sanidine and compositions near core-rim boundaries (Fig. 10c) are more calcic (up to $Ab_{65}An_{32}Or_3$, Fig. 9). Plagioclase in sieve-textured biotite is $Ab_{76}An_{20}Or_4$ (Table 4). In contrast, group II plagioclases (cores) have compositions clustering between $Ab_{68}An_{30}Or_2$ and $Ab_{56}An_{42}Or_2$ (Fig. 9, Table 4). A few cores have higher An contents and others are more sodic (Fig. 9). Overall, there is a clear compositional difference between groups I and II. No systematic variation of plagioclase composition with stratigraphic position has been found (Fig. 15).

Various plagioclase crystals were scanned for major elements. For an isolated group I plagioclase (Fig. 4b) the profile has several domains separated from each other by small compositional gaps (a few An %, Fig. 10a). Low-amplitude oscillatory zoning is superimposed. Several discrete stages of crystal growth can be recognized. In contrast, profiles for crystals with a group II core (Figs. 4d, e and 10b, c) show an abrupt compositional gap between core and rim coinciding with the optical boundary between the two parts of the crystal. The zonation and An contents in the rims is similar to that in group I crystals (Fig. 10a). Profiles in cores are symmetric, often "M"-shaped (Fig. 10b) and with low-amplitude fluctuations (Fig. 10c). The large difference in An content and the marked compositional break imply important changes of the crystallization conditions between core and rim. This raises the problem of the significance of plagioclase cores (see below).

The *biotite* chemistry (Tables 5 and 6) is characterized by elevated Al and Fe/(Fe+Mg), and appreciable contents of Ti, in agreement with Noble et al. (1984). Zn is also present in detectable amounts (Table 5, see also Montel et al. 1986b). F concentrations are variable (reaching levels in excess of 3.5 wt %, Table 5). This contrasts with the low values found by Noble et al. (1984). The Macusani biotites are generally similar to biotites from muscovite- or Al_2SiO_5-bearing granites (e.g., de Albuquerque 1973; Neiva 1976; Price 1983) or from high-grade metapelites (e.g., Blumel and Schreyer 1977; Gil Ibarguchi and Martinez 1982; Brown 1983). Structural formulae (Table 5) are characterized by elevated Al^{VI}, generally higher than 1 a./f.u., and these biotites lie outside of the phlogopite-annite-siderophyllite-eastonite plane. On the $M^{2+} - Al - Si$ diagram of Monier and Robert (1986b, Fig. 11), the biotites plot in positions intermediate between trioctahedral and dioctahedral micas. This indicates the presence of substantial octahedral vacancies. No clear variation in the biotite

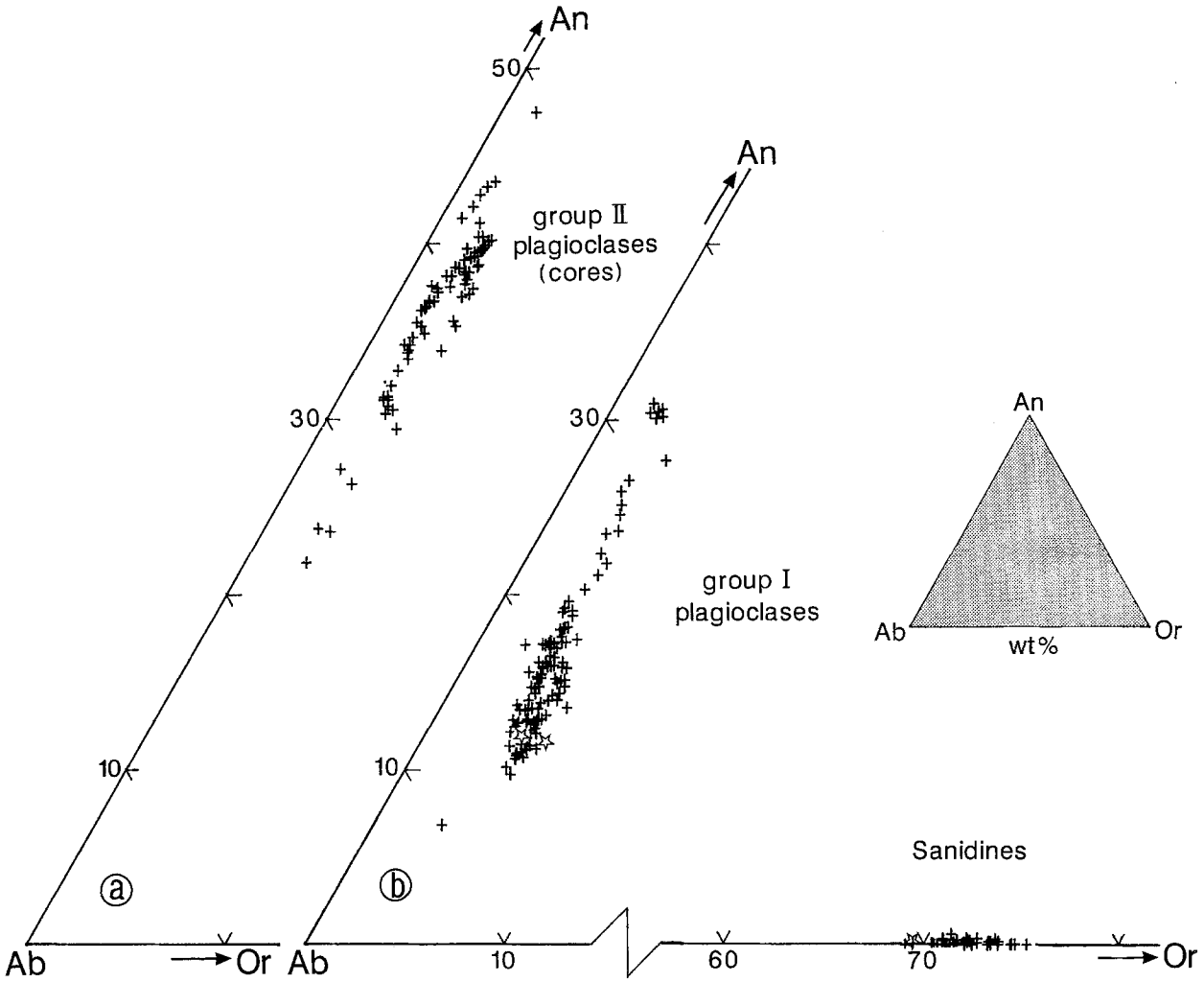

Fig. 9a, b. Compositions of feldspars in the Macusani tuffs and obsidian glasses. **a** group II plagioclases (cores); **b** sanidines and group I plagioclases; (☆): plagioclases and sanidines from glasses. Note that the number of data points is not representative of the proportion between the two types of plagioclase

chemistry with stratigraphic position can be demonstrated (Fig. 15). All biotites have closely similar compositions (Fig. 12), including sieve-textured biotites, inclusions in andalusite and plagioclase cores, biotite in glomerocrysts and obsidian glasses. Only rare, late crystallizing biotites from both tuffs and glasses show significant differences with the others (Fig. 12). The late biotites exhibit the largest shifts towards dioctahedral micas (Fig. 11) and have the highest F and the lowest Ti (e.g., n° 8 in Table 5). They define a negative Al^{VI} vs. Mg/(Mg+Fe) trend (Fig. 12). These variation trends (Figs. 11, 12) closely parallel those for biotites in leucogranites (e.g., Monier and Robert 1986b).

The *spinels* associated with the sieve-textured biotites are zincian hercynites with compositions ranging between $Hc_{61}Ga_{39}$ and $Hc_{51}Ga_{49}$ (Table 8). They have low calculated Fe^{3+}/Fe^{2+} (about 0.05, Table 8).

Muscovite (microprobe analyses (Table 5) and one muscovite separate from the Picotani field (Table 6)) contains significant Fe, Mg, Ti, Na and F and the compositions are similar to muscovites in two-mica granites (Miller et al. 1981; Monier et al. 1984; Monier and Robert 1986a). Our data compare well with those of Noble et al. (1984) except for F (see above). On the M^{2+} – Al – Si diagram (Fig. 11), they plot between the muscovite-biotite and the muscovite-celadonite lines, indicating the presence of both biotitic and phengitic substitutions (Monier and Robert 1986a). Again, there is no systematic evolution of muscovite composition with stratigraphic composition (Fig. 15), but there are variations with texture. Texturally-late muscovites have very low Ti and the highest F contents (Table 5, compare with similar trends for the biotites). They also plot the farthest from the ideal muscovite composition with significant phengitic substitution (Fig. 11). In contrast, earlier muscovites, with elevated Ti and lower F contents (Table 5), plot closer to ideal muscovite and are mostly affected by the biotitic substitution (Fig. 11). The use of coupled crystallochemical tests (C Ramboz, unpub.) indicates that the iron in analysed muscovites is dominantly Fe^{2+}, in agreement with the results of Monier and Robert (1986a) for muscovites from leucogranites. This contrasts with the very elevated Fe^{3+}/Fe^{2+} found by Miller et al. (1981), suggesting the possibility of secondary oxidation in their supposed primary leucogranitic muscovites. The evolution, from relatively early, high-temperature muscovites (with limited biotitic substitution) towards later, lower-temperature (more phengitic) compositions is consistent with the data of Monier and Robert (1986a) on muscovite solid solutions. Also, the noted decrease in Ti and increase in F agrees with trends re-

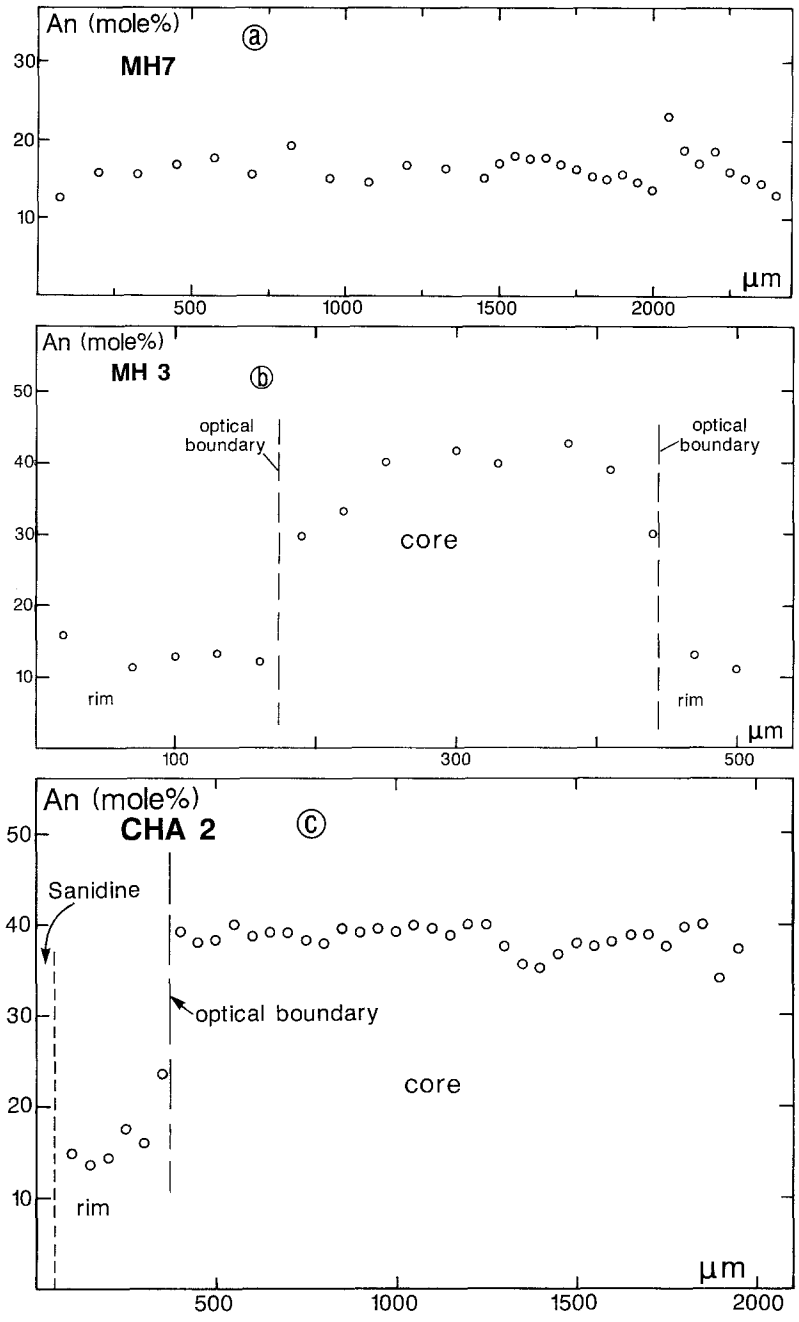

Fig. 10a–c. Microprobe traverses in plagioclase crystals; **a** group I plagioclase (Fig. 4b); **b** and **c** group II plagioclase cores with group I plagioclase rims (respectively Fig. 4e and d)

corded with fractionation in plutonic rocks (Miller et al. 1981; Monier et al. 1984; Monier and Robert 1986a). However, the relatively large compositional variations found here (for undoubtedly magmatic muscovites) means that muscovite composition probably cannot be reliably used as an indicator of either a "primary" or "secondary" origin (cf. Miller et al. 1981).

Microprobe analyses of *andalusite* and *sillimanite* (Table 7 and French and Meyer 1970; Noble et al. 1984) show that they are both close to Al_2SiO_5. Fluorine could not be detected in andalusite and ion microprobe analyses reveal only trace amounts of B and Li (ES Grew, written comm. 1986).

Tourmaline is essentially part of the schorl-dravite series (Table 7), but contains a significant amount of F and detectable Zn. Except for rare texturally-late crystals, the tourmaline compositions are quite uniform (cf. similar trends for biotite). There is no systematic variation in tourmaline composition with position in the sequence (Fig. 15). The evolution with progressive crystallization is marked by a decrease of both CaO and Mg/(Mg+Fe) (from 0.3–0.35 down to 0.05), while Al stays roughly constant. Strong chemical zonation is rare. The scanned crystals do not show any large variation in Mg/(Mg+Fe) except for narrow outer rims (Fig. 13). The tourmaline compositions and zoning types are similar to magmatic tourmalines from leucogranites and pegmatites (Power 1968; Neiva 1974; Manning 1982; Charoy 1986; Joliff et al. 1986) and to experimentally crystallized tourmalines from leucogranitic starting materials (Benard et al. 1985).

The *apatites* are nearly pure fluorapatites (Table 9), in agreement with the preliminary determinations of Noble

Table 5. Representative electron microprobe analyses of biotite (1–11) and muscovite (12–16)

	MH1	MH7	MH4	MH8	CEA 1	CHA 2	MH4	MH7		JV2		MH3	MH7	MH8	MH3	MH7
	1	2	3	4	5	6	7	8	9	10	11	12	13	14	15	16
SiO_2	37.25	35.69	35.61	35.06	36.09	35.65	36.49	36.99	35.86	34.72	36.78	46.06	45.73	45.03	46.43	44.47
Al_2O_3	20.74	20.23	20.18	19.73	19.76	19.25	20.02	22.61	20.66	20.08	22.08	34.78	33.90	35.74	34.20	32.41
FeO	19.39	20.68	22.67	23.30	21.28	21.68	21.18	19.77	18.74	22.35	20.18	2.63	2.74	1.48	2.56	3.35
MnO	0.12	0.07	0.16	0.11	0.16	0.13	0.15	0.34	n.d.	0.16	0.15	0.00	0.07	0.00	n.d.	0.04
MgO	4.72	6.39	5.16	5.50	5.31	5.43	5.27	5.34	6.54	4.20	2.02	1.13	1.08	0.91	1.06	1.08
CaO	0.00	0.00	0.00	0.00	0.01	0.00	0.00	0.01	0.00	0.00	0.00	0.00	0.00	0.00	0.01	0.00
Na_2O	0.32	0.58	0.42	0.49	0.50	0.43	0.28	0.45	0.45	0.38	0.57	0.69	0.67	0.57	0.64	0.67
K_2O	9.31	9.25	9.28	8.84	9.12	9.02	8.68	9.55	9.32	9.24	9.20	10.16	10.11	10.33	9.91	10.19
TiO_2	2.52	3.42	3.31	2.78	3.49	3.19	3.20	0.10	3.34	3.23	0.95	0.56	0.62	0.66	0.61	0.00
ZnO	0.00	0.03	0.07	0.38	0.14	0.00	0.50	0.21	n.d.	0.00	0.00	0.09	0.00	0.21	n.d.	0.01
F	n.d.	1.18	2.40	3.03	n.d.	n.d.	n.d.	3.61	n.d.	2.04	n.d.	1.50	1.66	0.68	n.d.	2.13
Total	94.37	97.52	99.26	99.22	95.86	94.78	95.76	98.98	94.91	96.40	91.93	97.60	96.58	95.61	95.42	94.35
$O \equiv F$	–	0.50	1.01	1.28	–	–	–	1.52	–	0.86	–	0.63	0.70	0.29	–	0.90
Total	–	97.02	98.25	97.94	–	–	–	97.46	–	95.54	–	96.97	95.88	95.32	–	93.45
Si	5.67	5.39	5.40	5.38	5.49	5.5	5.53	5.59	5.44	5.41	5.76	6.12	6.16	6.04	6.19	6.20
Al^{IV}	2.33	2.61	2.60	2.62	2.51	2.5	2.47	2.41	2.56	2.59	2.24	1.88	1.84	1.96	1.81	1.80
Al^{VI}	1.39	0.99	1.01	0.95	1.03	1.00	1.11	1.62	1.13	1.10	1.84	3.57	3.54	3.69	3.57	3.52
Ti	0.29	0.39	0.38	0.32	0.40	0.37	0.36	0.01	0.38	0.38	0.11	0.06	0.06	0.07	0.06	0.00
Fe	2.47	2.61	2.88	2.99	2.71	2.80	2.69	2.50	2.38	2.91	2.64	0.29	0.31	0.16	0.29	0.39
Mn	0.02	0.01	0.02	0.01	0.02	0.02	0.02	0.04	0.00	0.02	0.02	0.00	0.01	0.00	0.00	0.00
Mg	1.07	1.44	1.17	1.26	1.20	1.25	1.19	1.20	1.48	0.98	0.47	0.22	0.22	0.18	0.21	0.22
Zn	0.00	0.00	0.01	0.04	0.02	0.00	0.06	0.02	0.00	0.00	0.00	0.01	0.00	0.02	0.00	0.00
Ca	0.00	0.00	0.00	0.00	0.00	0.00	0.00	0.00	0.00	0.00	0.00	0.00	0.00	0.00	0.00	0.00
Na	0.09	0.17	0.12	0.15	0.15	0.13	0.08	0.13	0.13	0.11	0.17	0.18	0.17	0.15	0.17	0.18
K	1.81	1.78	1.80	1.73	1.77	1.77	1.68	1.84	1.80	1.84	1.84	1.72	1.74	1.77	1.69	1.81
F	–	0.56	1.15	1.47	–	–	–	1.73	–	1.01	–	0.63	0.70	0.29	–	0.94

Total Fe as FeO. Structural formulae calculated on the basis of 22 O. *1, 2*: isolated biotites; *3, 4*: large biotites; *5*: large biotite associated with spinels, (Fig. 5b, c); *6*: disrupted fragment of a large biotite associated with spinel, both included in plagioclase (Fig. 4d); *7*: biotite inclusion in andalusite (Fig. 6b); *8*: texturally-late biotite; *9*: biotite inclusion in muscovite; *10, 11*: biotites in Macusani glass; *12*: large isolated muscovite; *13*: isolated muscovite; *14*: large muscovite with sillimanite inclusions (Fig. 5e); *15*: muscovite with biotite inclusions; *16*: texturally-late muscovite. n.d. = not determined

et al. (1984). Apatite inclusions in biotites have lower F concentrations, possibly because they were mechanically isolated from the F-enriched, evolved liquid (Pichavant et al. 1987a). Fe/Mn in apatite does not vary systematically from core (inside the sillimanite and zircon inclusions) to rim, although some individual apatite crystals have lower Fe/Mn in their rims.

The *ilmenite* chemistry is characterized by: (1) erratic Mn/Fe ratios (even at the thin section scale, see also Noble et al. 1984); (2) a maximum of a few mole % Fe_2O_3 in solid solution; and (3) locally very elevated $MnTiO_3$ (up to 70 mol %) in solid solution (Table 8, see also Noble et al. 1984). Scanning for other elements revealed the presence of only small amounts of Nb and Zn (Table 8, column 5). Noble et al. (1984) noted that a number of ilmenites have a slight deficiency in divalent cations and a corresponding excess in Ti. We confirm this point and emphasize that it is independent of the Mn/Fe ratio (Fig. 14; Table 8; Noble et al. 1984, analysis 3d). These analyses indicate elevated summation deficiencies also, suggesting the presence of some H_2O. These compositions are close to pseudorutile (complex intergrowth of Fe hydroxides and Ti oxides developed by alteration and oxidation of ilmenite, Grey and Reid 1975; Frost et al. 1983; Grey et al. 1983). Indeed, textures indicative of incipient alteration of ilmenite can be recognized with the scanning electron microscope. These appear as patches, darker in back-scattered imaging than the unaltered part of the crystals, but chemically indistinguishable from it. We interpret the peculiar chemistry of some Macusani ilmenites (Fig. 14) as due to partial alteration and oxidation. Phases without any apparent excess Ti are considered representative of the chemistry of magmatic ilmenites.

The *niobian rutiles* (derived by biotite decomposition) contain elevated Sn and W and negligible Ta and Mn (Table 8). This contrasts with the ilmenite composition (low to moderate Nb, Sn, W, Ta, high Mn) but reflects, in part, the trace element chemistry of the parent mica (Table 6). Phases with comparable compositions are known from rare-element pegmatites (e.g., Černý et al. 1986).

Both *zircon* and *monazite* have elevated U contents (zircon: 0.5–3.5 wt %; monazites: 1.0–1.5 wt % UO_2) and monazite has elevated Th contents (4.0–7.5 wt % ThO_2).

Interpretation of the mineralogical data and magmatic evolution

From textural evidence summarized in Fig. 3, the mineral assemblage may be divided into two groups: early and later phases. The early phases include the group II plagioclases,

Table 6. Chemical analyses of biotite (1–5) and muscovite (6) mineral separates from the Macusani volcanics

	323	325	327	330	TsVm1[a]	
	1	2	3	4	5	6
SiO_2	36.48	35.64	35.54	36.35	34.62	44.80
Al_2O_3	19.22	19.65	19.87	20.32	19.23	35.60
Fe_2O_3	19.06	8.27	6.76	7.28	2.99	1.32[b]
FeO	4.86	14.37	15.37	14.67	20.66	–
MnO	0.21	0.17	0.22	0.31	0.14	0.05
MgO	4.72	5.26	4.43	4.09	5.25	0.10
CaO	0.30	0.15	0.29	0.13	0.11	0.12
Na_2O	0.61	0.47	0.70	0.71	0.49	0.80
K_2O	8.32	8.60	8.53	8.70	8.63	8.87
TiO_2	3.20	3.16	2.92	2.63	3.35	0.28
P_2O_5	0.15	0.07	0.19	0.09	0.05	–
Total	97.13	95.81	94.82	95.28	95.52	91.94
Ba	322	510	252	335	249	85
Rb	1534	1424	1854	2093	1624	1459
Sr	5	0	5	0	0	6
Zr	154	153	211	136	89	–
Nb	157	130	204	189	137	–
Cr	87	60	59	36	50	–
V	273	258	219	203	241	

Analyses carried out at Queen's University, Kingston, Ontario by X-ray fluorescence; Fe^{2+} and Fe^{3+} determined by titration (Kontak 1985)

[a] From the Picotani field
[b] Total Fe as Fe_2O_3

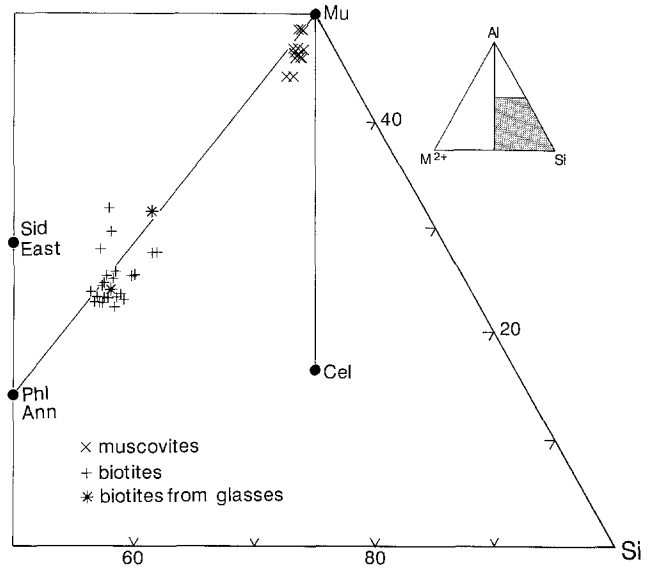

Fig. 11. Al (Al+Fe^{3+}−2Ti) − M^{2+} (Fe^{2+}+Mg+Mn+Ti) − Si (Si+2Ti) diagram (cations per formula unit, Monier and Robert 1986a, b) showing the compositions of the micas in the Macusani volcanics. Mica compositions are plotted assuming Fe^{3+} = 10 mol% total Fe. *Mu*: muscovite; *Cel*: celadonite; *Phl*: phlogopite; *Ann*: annite; *Sid*: siderophyllite; *East*: eastonite

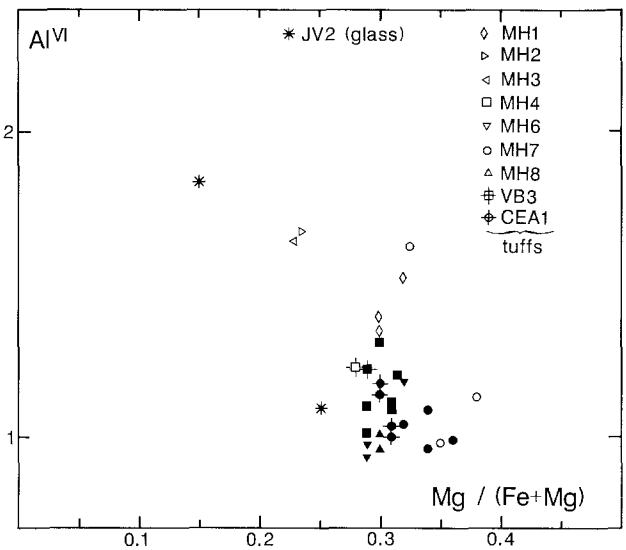

Fig. 12. Al^{VI} vs Mg/(Fe+Mg) (cations per formula unit) for biotites in the Macusani volcanics. *Open symbols*: texturally-late biotites; *filled symbols*: texturally-early biotites

most of the biotites and tourmalines, spinel, the cordierite-type phases, sillimanite and most of the accessories (ilmenite, apatite, monazite and zircon). The later phases are: quartz, sanidine, the group I plagioclases, muscovite, andalusite, niobian rutile, a minor proportion of the biotites and tourmalines and of the accessories. Each group of phases possesses strongly contrasting features (i.e., andalusite instead of sillimanite, group I vs. group II plagioclases). This enables a distinction to be made between an early and a main magmatic stage; below we discuss the significance of each.

Early magmatic phases: restites, xenocrysts or phenocrysts?

The early phases might be considered, alternatively, as early phenocrysts (precipitates from the melt), restites (residual source crystals) or xenocrysts (foreign magmatic crystals, the lithic fragments being excluded). Textural criteria and chemical data allow us to discriminate between these different possibilities.

White and Chappell (1977) and Chappell et al. (1987) proposed that most of the plagioclase cores in granitic and volcanic suites represent restites. The An-rich compositions of the group II plagioclases from this study (for a Ca-poor rhyolitic bulk rock composition, see Noble et al. 1984; Valencia Herrera et al. 1984; Pichavant et al. 1988) and the large compositional contrast between plagioclases from groups I and II are compatible with such an hypothesis. However, the textures and chemical zonation (Figs. 4 and 10) are clearly igneous features. Restitic plagioclase crystals from high grade metasediments would not exhibit these features. In particular, chemical zonation would be absent or weak (e.g., Smith and Brown 1987). On the other hand, high temperature plagioclases crystallizing in granitic or rhyolitic magmas are An-rich, even for low to moderate bulk CaO contents (e.g., Ewart 1963; Clemens et al. 1986; Wall et al. 1987). For example, liquidus plagioclase crystallizing in the system Qz − Or − Ab − An with 5 wt % An (i.e., 1 wt % CaO) at 3 kbar P_{H_2O}, 720° C has a composition close to An_{35} (Weber and Pichavant 1986; in prep.). In addition, there is no reason to consider these plagioclases

Table 7. Representative electron microprobe analyses of tourmaline (1–6), cordierite-type phases (7–8), andalusite (9–11) and sillimanite (12–13)

	MH3	MH7	MH1	CEA 1		MH2	MH4	MH6	MH4		JV1	MH3	MH8
	1	2	3	4	5	6	7	8	9	10	11	12	13
SiO_2	34.77	34.93	36.47	34.50	34.93	34.62	50.41	52.78	36.69	36.89	38.17	36.66	36.14
Al_2O_3	34.65	35.07	33.99	34.63	34.05	34.31	33.95	18.60	61.77	62.21	62.44	63.14	63.52
FeO	11.10	10.29	9.74	9.59	12.71	11.89	3.61	13.35	0.29	0.25	0.19	0.21	0.14
MnO	0.07	0.00	0.12	n.d.	n.d.	0.29	0.00	0.00	0.06	0.00	0.04	0.00	0.10
MgO	3.07	3.04	3.11	3.51	1.70	0.89	0.36	1.89	0.05	0.05	0.01	0.00	0.04
CaO	0.22	0.13	0.28	0.33	0.10	0.14	0.86	2.32	0.00	0.02	0.00	0.00	0.04
Na_2O	2.10	1.94	1.95	2.07	2.14	1.96	0.16	0.06	0.00	0.00	0.00	0.00	0.00
K_2O	0.09	0.06	0.00	0.04	0.03	0.00	0.21	0.27	0.00	0.00	0.00	0.00	0.00
TiO_2	0.82	0.33	0.82	0.99	0.87	0.69	0.00	0.00	0.08	0.00	0.03	0.05	0.00
ZnO	0.22	0.32	0.00	n.d.	n.d.	0.10	n.d.	n.d.	n.d.	n.d.	n.d.	n.d.	n.d.
F	0.73	0.63	n.d.	n.d.	n.d.	n.d.	n.d.	n.d.	n.d.	n.d.	n.d.	n.d.	n.d.
Total	87.84	86.74	86.48	85.66	86.53	84.89	89.56	89.26	98.94	99.42	100.88	100.06	99.98
O≡F	0.31	0.27	–	–	–	–	–	–	–	–	–	–	–
Total	87.53	86.47	–	–	–	–	–	–	–	–	–	–	–
Si	5.74	5.79	5.98	5.74	5.83	5.87	–	–	1.00	1.00	1.02	0.99	0.98
Al	6.74	6.85	6.57	6.79	6.70	6.85	–	–	1.99	1.99	1.97	2.01	2.02
Ti	0.10	0.04	0.10	0.12	0.11	0.09	–	–	0.00	0.00	0.00	0.00	0.00
Fe	1.53	1.43	1.34	1.33	1.77	1.68	–	–	0.01	0.01	0.00	0.00	0.00
Mg	0.76	0.75	0.76	0.87	0.42	0.22	–	–	0.00	0.00	0.00	0.00	0.00
Mn	0.01	0.00	0.02	–	–	0.04	–	–	0.00	0.00	0.00	0.00	0.00
Zn	0.03	0.04	0.00	–	–	0.01	–	–	0.00	0.00	0.00	0.00	0.00
Ca	0.04	0.02	0.05	0.06	0.02	0.03	–	–	0.00	0.00	0.00	0.00	0.00
Na	0.67	0.62	0.62	0.67	0.69	0.64	–	–	0.00	0.00	0.00	0.00	0.00
K	0.02	0.01	0.00	0.01	0.01	0.00	–	–	0.00	0.00	0.00	0.00	0.00
F	0.38	0.33	–	–	–	–	–	–	0.00	0.00	0.00	0.00	0.00

Total Fe as FeO. Structural formulae calculated on the basis of 24.5 O (tourmalines), 5 O (Al-silicates). *1*: isolated tourmaline with sillimanite inclusions; *2*: isolated tourmaline; *3*: tourmaline inclusion in plagioclase; *4*: isolated tourmaline, core (Figs. 6f and 13); *5*: same tourmaline, rim (Fig. 13); *6*: texturally late tourmaline; *7*: cordierite-type phase; *8*: cordierite-type phase; *9*: isolated andalusite, colourless rim (Fig. 6a); *10*: same andalusite, pink core (Fig. 6a); *11*: andalusite, Macusani glass; *12*: sillimanite inclusion in sanidine; *13*: sillimanite inclusion in muscovite (Fig. 5e). n.d. = not determined

as xenocrysts; the Macusani volcanics are presently not known to show any relation with exposed basaltic or andesitic volcanism and they lack foreign igneous inclusions. Phases considered as likely xenocrysts in felsic peraluminous magmas, such as olivine, pyroxenes and amphiboles are absent. The biotite composition is very homogeneous and there is no indication of the presence of chemically distinct biotites. This argues against a xenocrystic origin for the plagioclase cores. The chemical and isotopic data (Kontak et al. 1984a; Noble et al. 1984; Pichavant et al. 1987a, 1988) exclude any important mixing with non-crustal components during magma genesis. The most likely explanation is, therefore, to consider these plagioclase cores as high temperature, early magmatic phenocrysts.

In the same way, biotite, mostly associated with the early magmatic stage, may be viewed either as restitic, xenocrystic or as an early phenocryst. The sieve-textured biotites associated with spinels are similar to those from xenoliths in basic rocks (e.g., Lacroix 1893; Maury and Bizouard 1974; Brearley 1987a) and to experimentally-reacted biotites (Brearley 1987b). These textures are produced by disequilibrium melting of biotite (Brearley 1987a, b). Partitioning of Zn between biotite (see Montel et al. 1986b for detailed Zn analyses in biotite) and spinel is consistent with such a reaction (Montel et al. 1986b). Since these textures are early in the magmatic history (see above), they can not result from processes occurring at shallow levels such as magma degassing (Grant 1985). The inescapable conclusion is therefore that partial melting of biotite occurred at depth. One possibility is that these biotites represent partially reacted fragments of pelitic materials incorporated during magma ascent and therefore are xenocrystic. However, the Macusani volcanics are virtually free of pelitic xenoliths of deep provenance, implying that assimilation was not important during magma ascent. As the Macusani magmas are low to moderate temperature (see below) felsic magmas, they would have little ability to assimilate foreign materials. In addition, there is no difference between the composition of sieve-textured biotites and of other biotites (see above and Fig. 12), as would be expected if incorporation of pelitic materials has taken place at different crustal levels en route to the surface. Therefore, the only possibility remaining is that the sieve-textured biotites come from the source region of the Macusani magmas. These (and the associated spinels) must be considered as true restites. The disequilibrium melting textures and reaction products probably result from locally rapid elevations in temperature in the source region. We emphasize that we do not imply that

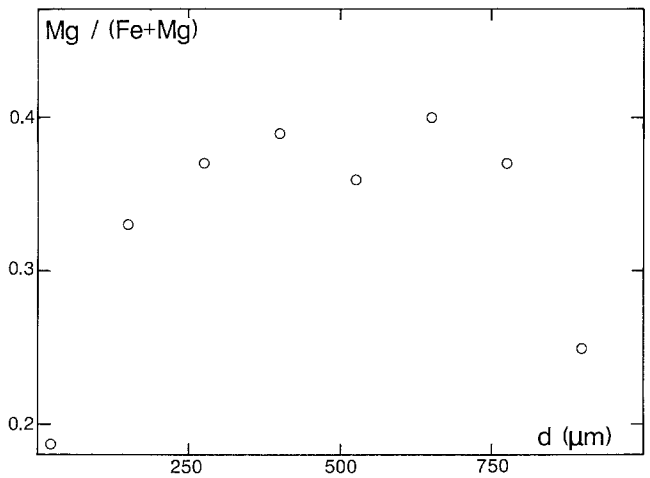

Fig. 13. Variations in Mg/(Fe+Mg) (cations per formula unit) in tourmaline (microprobe traverse of Fig. 6f). Note the nearly constant Mg/(Fe+Mg) composition except for a narrow outer rim

all biotites are restites. There is no ambiguity for the texturally and chemically late biotites from the main magmatic stage (see above): these are clearly phenocrysts.

The cordierite-type phases and much of the tourmaline may be alternatively interpreted as restitic or early magmatic phenocrysts. Decisive evidence is lacking for cordierite-type phases, although rare textures (Fig. 5d) suggest that

Table 9. Representative electron microprobe analyses of apatite

	MH2		MH4	MH8
	1	2	3	4
FeO	0.73	0.59	1.00	0.71
MnO	0.57	0.93	0.83	0.84
CaO	53.96	53.01	54.02	54.48
P_2O_5	42.77	41.43	42.04	41.11
La_2O_3	0.13	0.11	0.00	0.00
Ce_2O_3	0.23	0.15	0.03	0.15
F	4.06	3.77	3.19	3.89
Cl	0.08	0.00	0.00	0.00
Total	102.54	99.99	101.09	101.18
O≡F, Cl	1.71	1.59	1.34	1.64
Total	100.83	98.40	99.75	99.54
Ca	4.81	4.86	4.90	4.96
Fe	0.05	0.04	0.07	0.05
Mn	0.04	0.07	0.06	0.06
P	3.02	3.00	3.02	2.96
La	0.00	0.00	0.00	0.00
Ce	0.01	0.01	0.00	0.01
F	1.07	1.02	0.86	1.05
Cl	0.01	0.00	0.00	0.00

Total Fe as FeO. Structural formulae calculated on the basis of 13 anions. *1*: isolated apatite, core (Fig. 8a); *2*: same crystal (Fig. 8a), rim; *3*: apatite inclusion in biotite; *4*: isolated apatite

Table 8. Representative electron microprobe analyses of ilmenites (1–5), niobian rutiles (6–7) and spinels (8–11)

	MH2	MH3				MH3		MH6	CEA 1		
	1	2	3	4	5	6	7	8	9	10	11
Al_2O_3	n.d.	0.00	0.00	0.00	n.d.	n.d.	n.d.	55.79	56.44	56.44	56.23
FeO	41.80	12.42	45.29	46.30	36.39	1.40	1.97	24.29	20.80	22.05	24.34
MnO	4.42	33.26	2.59	1.77	1.67	0.00	0.00	0.08	0.17	0.17	0.11
MgO	0.10	0.26	0.10	0.15	0.35	0.02	n.d.	1.24	1.10	1.08	1.08
TiO_2	52.74	54.55	51.06	52.27	57.71	93.06	92.86	0.00	0.06	0.20	0.00
NiO	0.04	0.00	0.04	0.00	0.00	0.00	n.d.	n.d.	n.d.	n.d.	n.d.
Cr_2O_3	0.00	0.00	0.00	0.25	0.00	0.00	n.d.	n.d.	n.d.	n.d.	n.d.
ZnO	0.00	n.d.	n.d.	n.d.	0.17	0.00	n.d.	16.48	21.08	19.82	16.72
WO_3	n.d	n.d.	n.d.	n.d.	0.00	1.45	2.61	n.d.	n.d.	n.d.	n.d.
SnO_2	n.d.	n.d.	n.d.	n.d.	0.00	2.05	2.20	n.d.	n.d.	n.d.	n.d.
Ta_2O_5	n.d.	n.d	n.d.	n.d.	0.00	0.00	0.00	n.d.	n.d.	n.d.	n.d.
Nb_2O_5	n.d.	n.d.	n.d.	n.d.	0.22	0.50	0.44	n.d.	n.d.	n.d.	n.d.
Total	99.06	100.49	99.04	100.74	96.81	98.46	100.08	97.88	99.65	99.76	98.48
Al	–	–	–	–	–	–	–	15.76	15.76	15.73	15.80
Ti	2.01	2.03	1.97	1.98	2.18	0.971	0.964	0.00	0.01	0.04	0.00
Fe^{3+}	0.00	0.00	0.09	0.06	0.00	0.000	0.000	0.23	0.21	0.18	0.19
Fe^{2+}	1.78	0.52	1.85	1.89	1.54	0.016	0.016	4.64	3.91	4.18	4.67
Mn	0.19	1.40	0.11	0.08	0.07	–	–	0.02	0.03	0.03	0.02
Mg	0.01	0.02	0.01	0.01	0.03	–	–	0.44	0.39	0.38	0.38
Zn	–	–	–	–	0.02	–	–	2.92	3.69	3.46	2.94
W	–	–	–	–	–	0.005	0.009	–	–	–	–
Sn	–	–	–	–	–	0.012	0.012	–	–	–	–
Nb	–	–	–	–	0.00	0.002	0.002	–	–	–	–

Total Fe as FeO. Structural formulae calculated on the basis of 6 O (ilmenites), 2 O (niobian rutiles) and 32 O (spinels). Fe^{3+} calculated from site occupancy considerations. *1*: ilmenite inclusion in apatite (Fig. 8a, b); *2, 3, 5*: ilmenite inclusions in biotites; *4*: ilmenite inclusion in feldspar; *6, 7*: niobian rutiles; *8–11*: spinels associated with sieve-textured biotites (Fig. 5b, c). n.d. = not determined

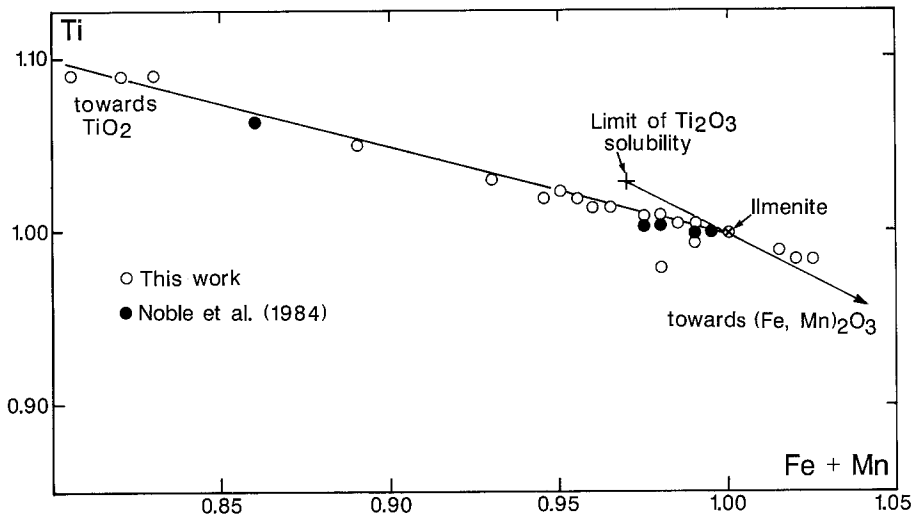

Fig. 14. Ti vs. (Fe+Mn) (cations per formula unit) showing the compositions of ilmenites in the Macusani ash-flow tuffs. The limit of Ti_2O_3 solubility is after Grey et al. (1974). The *solid line* drawn corresponds to Ti=2 (Fe+Mn). See text for explanations

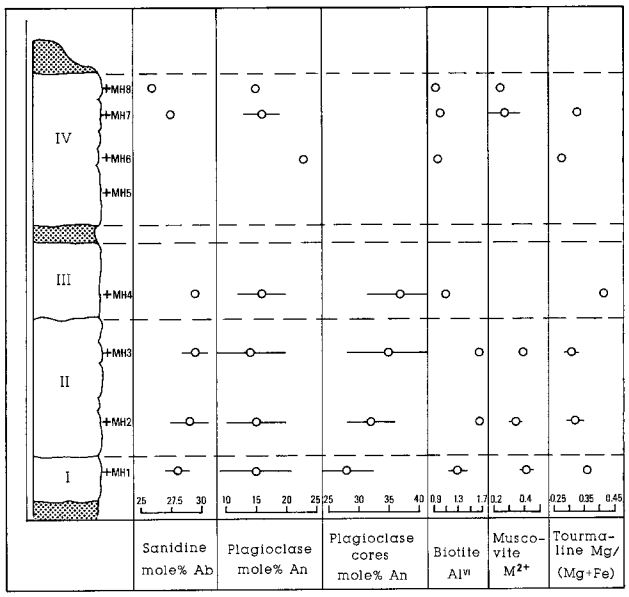

Fig. 15. Variation in mineral chemistry with stratigraphic position across the Huiquiza section. Data in cations per formula unit except for feldspars. In muscovite, $M^{2+} = Fe^{2+} + Mg + Mn + Ti$ (see caption of Fig. 11 and text). The data plotted are average values (calculated from the data base for each sample) and the error bar is the calculated standard deviation for each population

they are breakdown products of biotite and therefore in part restitic. Tourmalines of the schorl-dravite series have important thermal stability (Robbins and Yoder 1962; Manning 1981; Benard et al. 1985). The weak optical/chemical zonations, the compositions and colours of the Macusani tourmalines are consistent with crystallization at high temperatures (e.g., Benard et al. 1985). However, in absence of textural criteria, it is impossible to discriminate between a restitic or an early magmatic origin for tourmaline. Nevertheless, the few late crystallizing tourmalines are clearly phenocrysts.

A number of textures (strongly heterogeneous distribution of sillimanite inclusions, presence of coarse, prismatic, sillimanite crystals) suggests that some sillimanite is restitic. The high normative corundum of the volcanics (from >2 up to more than 5%, Barnes et al. 1970; Noble et al. 1984; Valencia Herrera et al. 1984; Pichavant et al. 1987a, 1988) also supports the presence of restitic sillimanite, on the basis of the experimental data of Clemens and Wall (1981). In contrast, other textures and habits (the zonally distributed sillimanite needles) more likely suggest magmatic crystallization of sillimanite. Therefore, sillimanite is considered to be in part residual and for the other part early magmatic. Partial melting occurred with sillimanite in excess to saturate the melt. Magmatic sillimanite later crystallized from the Al_2SiO_5-saturated melt.

Although decisive textural criteria are lacking for apatite (and also for ilmenite, monazite and zircon), P_2O_5 contents (0.2–0.4 wt %, Noble et al. 1984; Valencia Herrera et al. 1984; Pichavant et al. 1987a, 1988) are much higher than for apatite saturation at 800° C: 225 ppm (Harrison and Watson 1984). The ash-flow tuffs are also largely oversaturated with monazite (Montel 1986). These features suggest that restitic apatite and monazite should be present. In contrast, Zr concentrations in the tuffs (average 70 ppm, Noble et al. 1984; Pichavant et al. 1987a, 1988) are generally lower than zircon solubility for peraluminous granite compositions (about 100 ppm, Watson and Harrison 1983). Thus, most of the zircons should be phenocrysts rather than restites, in agreement with the small number of observed zircon cores.

Significance of the early magmatic stage and intensive parameters

From the above discussion, we conclude that the mineral phases associated with the early magmatic stage include both true restites and early phenocrysts. It is emphasized that the restite content of the magmas must be low (see Fig. 2 for the modal proportions) and may be estimated at a maximum of 5 vol. %. The early mineral association is assumed to preserve evidence of the magmatic evolution at or near the source region (i.e., partial melting and crystallization of early phenocrysts). The early phases may now be used to constrain the lithology of the source rocks (Pichavant et al. 1988) and to bracket the intensive parameters during the early magmatic stage.

First-order constraints on the $P - T$ conditions during the early magmatic stage are furnished by the andalusite-sillimanite transition (Holdaway 1971), the "muscovite out" univariant equilibrium for pure OH-muscovite and

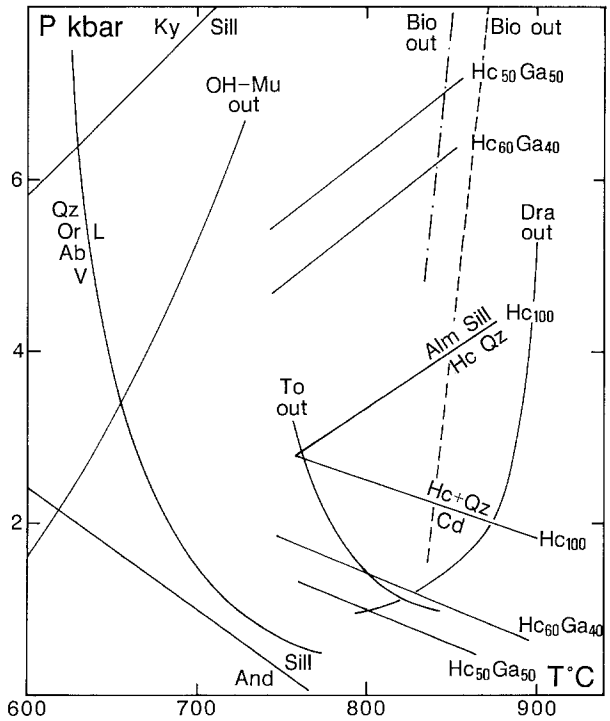

Fig. 16. $P - T$ conditions during the early magmatic stage. H_2O-saturated granite solidus (Qz Or Ab V = L) from Luth (1976), *Qz* = quartz; *Or* = K-feldspar; *Ab* = albite; *V* = pure H_2O fluid phase; *L* = silicate melt. Al_2SiO_5 equilibria from Holdaway (1971), *And* = andalusite; *Sill* = sillimanite; *Ky* = kyanite. Muscovite-out curve (*OH – Mu out*) from Chatterjee and Johannes (1974). Fe – Zn hercynite reactions from Montel et al. (1986b). *Alm* = almandine; *Hc* = hercynite; *Ga* = gahnite; *Cd* = cordierite. The reactions are labelled with the spinel composition (mole %). Tourmaline-out curves (Fe – Mg tourmaline: *To out*; dravite: *Dra out*) from Benard et al. (1985) and Robbins and Yoder (1962) respectively. Biotite melting curves (*Bio out*): *dashed*: fluid absent, quartz-saturated phlogopite melting (Bohlen et al. 1983); *dashed-dotted*: $H_2O - CO_2$ fluid-present, quartz-saturated phlogopite melting (Bohlen et al. 1983)

the tourmaline out curves (Fig. 16). The following model biotite melting reaction:

biotite + sillimanite ± quartz and feldspars (1)
⇋ melt + spinel ± cordierite-type phases

may account for the biotite melting textures discussed above. A chemographic analysis of similar biotite-sillimanite-spinel reactions is given by Montel et al. (1986b). Application of the $Mg/(Fe^{2+} + Fe^{3+})$ ratios of coexisting biotite and spinel (Brearley 1987a) to the Macusani samples yield temperatures close to 800° C. Because the disequilibrium melting textures imply rapid heating rate in the source region (see above), these 800° C values must be considered as peak temperatures. 800° C is compatible with the stability field of spinel (Fe – Zn) plus quartz (e.g., Montel et al. 1986b). It is close to the temperatures given by phlogopite melting equilibria (Bohlen et al. 1983, Fig. 16, dashed lines) and intermediate between the two tourmaline out curves represented on Fig. 16. This temperature range is not unrealistically high given the high Ti and F contents in the Macusani biotites (which would tend to enhance their stability) and would be compatible (Olesch and Seifert 1981) with the possible presence of osumilite in the Macusani tuffs (see above).

Montel et al. (1986b) have constructed a petrogenetic grid for the appearance of hercynitic spinel from biotite-sillimanite assemblages. The breakdown of biotite-sillimanite to hercynitic spinel is restricted to an intermediate $P - T$ domain bounded towards the high pressures by breakdown reactions to garnet, and towards the low pressures by breakdown reactions to cordierite (Montel et al. 1986b; see also Fig. 16). This is illustrated in Fig. 16: the stability of Fe – Zn hercynite ($Hc_{60}Ga_{40}$, Table 8) + quartz is restricted to pressures below 5.5 kbar at 800° C. As an attempt to constrain pressure during the early magmatic stage, we have adapted the procedure of Nicholls et al. (1971, see Appendix). The regions of possible values of $a^L_{SiO_2}$ (Fig. 18) define a pressure range comprised between 3 and 5 kbar when calculations are carried out with thermochemical data for sillimanite from Robie et al. (1978). Although the errors are difficult to estimate, they are presumably large given the uncertainties on thermochemical data, activity models and phase compositions (Appendix). As an example, calculations using thermochemical data for sillimanite from Bohlen et al. (1986) furnish a wider range of pressure between 7.5 kbar and a negative pressure (Fig. 18). Nevertheless, the range of pressure obtained implies that magma generation took place in the mid-crust.

Ilmenite compositions (with a maximum of 3 mole % hematite component) suggest fo_2 conditions intermediate between the QFM and WM buffers (Lindsley, in Powers and Bohlen 1985). This is consistent with the low Fe^{3+}/Fe^{2+} of zincian hercynites (Table 8).

Several lines of evidence suggest values of $a_{H_2O} \ll 1$ during the early magmatic stage: (1) absence of muscovite in the source region and textural evidence of partial melting of biotite (e.g., Powers and Bohlen 1985); (2) high F/OH ratios in biotite, tourmaline and apatite, implying low f_{H_2O}/f_{HF} (Munoz and Ludington 1974; Korzhinskiy 1981); (3) the possible presence of osumilite (Olesch and Seifert 1981). From $P - T$ conditions inferred above, a_{H_2O} may be estimated by assuming that the solidus of the source rocks is approximately that of the Qz – Ab – Or system. Taking 800° C and 5 kbar as conditions of partial melting, one obtains a value of a_{H_2O} of 0.45 (Clemens and Vielzeuf 1987). The undoubted vertical mobility of the Macusani magmas reflects H_2O-undersaturated conditions during partial melting (e.g., Burnham 1979a).

Crystallization during the main magmatic stage

The transition from the early magmatic to the main magmatic stage is marked by major changes in mineralogy and mineral chemistry. Plagioclase composition changes abruptly from about An_{30-40} to An_{10-20} (see above) and quartz, sanidine and muscovite appear in the crystallization sequence. The change in plagioclase composition is nearly contemporaneous with the beginning of crystallization of andalusite. Although andalusite and sillimanite are both present in most samples (see above), the lack of a reaction relationship and the marked textural differences between the two imply a rapid change of the magmatic $P - T$ conditions from the sillimanite field to the andalusite field. The isolated andalusites represent phenocrysts in textural equilibrium with the melt whereas the sillimanite inclusions preserve earlier magmatic $P - T$ conditions. The mineralogical

Table 10. Fugacities of the main volatile species during crystallization of the Macusani magmas (calculations made for $T = 650°$ C, see Appendix)

Muscovite[a] no.	a_{Mu}^{WM}	f_{H_2O}[b] (bar)	f_{H_2O}[c] (bar)	a_{H_2O}[b]	a_{H_2O}[c]	H_2O melt[b] (wt %)	H_2O melt[c] (wt %)	$\log(f_{H_2O}/f_{H_2})$[b]	f_{H_2}[b] (bar)	$\log(f_{H_2O}/f_{HF})$[b]	f_{HF}[b] (bar)
12	0.50	1044	1052	>1	0.98	5.4	5.6	0.794	168	2.885	1.4
13	0.48	1002	1010	>1	0.94	5.4	5.4	0.794	161	2.823	1.5
14	0.67	1398	1410	>1	>1	5.4	5.7	0.794	225	3.288	0.7
16	0.41	856	863	0.90	0.80	4.9	4.7	0.794	138	2.690	1.7

[a] From Table 5
[b] Calculated for P = 1500 bar
[c] Calculated for P = 1750 bar

evidence therefore supports an abrupt change in $P - T$ conditions from the early to the main magmatic stage. We interpret this is as indicating rapid ascent of the magmas from their source regions. The incoming magmas may be viewed as dilute, crystal-poor suspensions of early phenocrysts and restites. The magmas were presumably stocked in "chambers", although we have no detailed information on their shape and size. The absence of important and systematic mineralogical (Figs. 2, 15) and geochemical (Pichavant et al. 1988) variations indicates that the different magma batches were largely independent from each other. This suggests separate magma "chambers", in space or time. According to modal proportions (Fig. 2), the percentage of crystallization is more important during that stage than during the early magmatic stage.

The coexistence of muscovite and andalusite throughout the volcanic field and the control on their respective modal proportions may be accounted for by the following multivariant equilibrium (in presence of melt):

$$\text{muscovite} + \text{quartz} \leftrightharpoons \text{sanidine} + \text{andalusite} \quad (2)$$

The variable modal proportions of muscovite and andalusite in the tuffs are attributed to changes in $P - T - a_{H_2O}$ conditions and muscovite composition (the F content is probably the most important as shown below). These changes might alternatively favour the right or the left-hand term of the reaction. For example, the ash-flow tuffs of the Picotani field contain muscovite but no andalusite (Mottet and Pichavant unpub. data), implying either lower temperatures, higher pressures, higher a_{H_2O} or higher F contents in muscovite than in the Macusani field (see Fig. 17). On the other hand, muscovite is absent from the obsidian glasses. These glasses were continuously degassed at progressively lower pressures up to the surface (Pichavant et al. 1987a), and were thus in the andalusite stability field. Assuming that muscovite coexisted with andalusite in the parental liquid, it was probably resorbed during degassing. From the crystallization order (muscovite postdates andalusite and some of the sanidine, Fig. 3), reaction (2) proceeded from right to left during crystallization of the Macusani magmas.

The marked difference between the composition of plagioclase cores and rims suggests a temperature drop from the early to the main magmatic stage. Cotectic plagioclases crystallized in the system Qz – Or – Ab – An with 5 wt % An (i.e., 1 wt % CaO) at 3 kbar P_{H_2O}, 660–670° C, have compositions close to An_{20} (Weber and Pichavant 1986; in prep.). Application of the two-feldspar thermometer (Brown and Parsons 1981) to sanidine-plagioclase group I pairs yield very low values of around 550° C. 2V angles of sanidine suggest temperatures close to 650° C (Smith and Brown 1987). From experimental data, the temperature during crystallization of such F-, B- and Li-rich magmas ranges below 700° C. H_2O-saturated liquidus temperatures of obsidian glasses are 650–625° C for 1–2 kbar (London et al. 1986; Boher et al. 1987, Fig. 17). The solidi of granitic rocks compositionally close to the Macusani glasses (the Harding pegmatite; Burnham and Nekvasil 1986; the Beauvoir granite, Boher et al. 1987; Pichavant et al. 1987b, Fig. 17) are lower than 650° C. These data consistently locate temperatures of crystallization at 650° C or lower during the main magmatic stage. For this temperature range, the presence of andalusite implies lithostatic pressures close to 1.5–2 kbar. These $P - T$ conditions appear inconsistent with the *stable* presence of virgilite in the Macusani glasses (London 1984; Fig. 17).

Fugacities of the main volatile species (H_2O, H_2, HF) and a_{H_2O} during the main magmatic stage may be calculated from the $P - T$ conditions inferred above (Appendix). This is made possible because of the presence of muscovite (and sanidine) phenocrysts of preserved magmatic chemistry. The results (Table 10) show a_{H_2O} to be around 1 (compare with value for the early magmatic stage). Plagioclase-liquid equilibria (Kudo and Weill 1970) yield H_2O pressures just above 1 kbar for the tuffs (650° C, plagioclase An_{15}, groundmass composition approximated by bulk rock composition MH3 from Pichavant et al. 1988). Therefore, calculations consistently imply that crystallization of the Macusani magmas occurred under near H_2O-saturation. The computed H_2O activities correspond to melt H_2O contents between 4.7 and 5.7 wt % (Table 10), in the upper range of values possible for silicic magmas at low pressures (Burnham 1979b; Blake 1984). These elevated H_2O contents may explain why fractional crystallization is not in a very advanced stage in the volcanic products. The system could not suffer a major increase in melt H_2O content (that would go along with extensive crystallization) without being erupted. A notable, although volumetrically minor, exception is represented by the obsidian glasses, residual liquids from the crystallization of the tuffs (Pichavant et al. 1987a, 1988). These glasses are probably derived from magma batches initially drier than the others.

The location, in $P_{H_2O} - T$ space, of the equilibrium A-5 (see Appendix) is shown for two muscovites representative of the range of F concentrations observed (Table 5). The two muscovite out reactions (Fig. 17) enclose the $P - T$

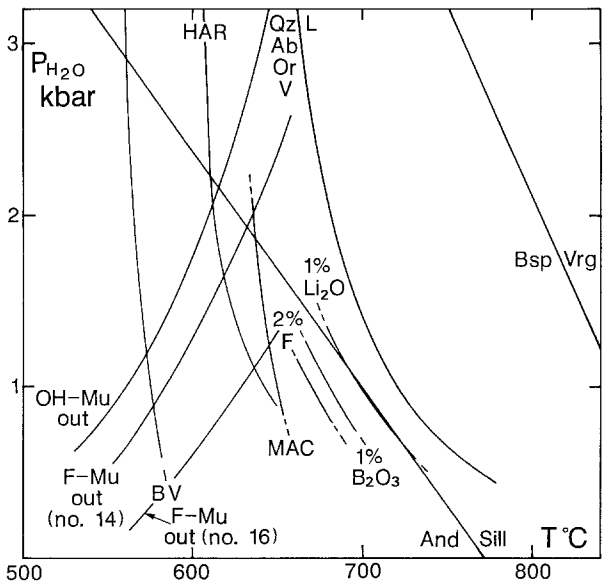

Fig. 17. $P_{H_2O} - T$ conditions during the main magmatic stage. Granite solidus, Al_2SiO_5 equilibria and OH – Mu out curve as in Fig. 16. The two muscovite out curves for F-bearing compositions (F – Mu out) are calculated (see Appendix). Virgilite (Vrg)-Betaspodumene (Bsp) transition from London (1984). Minimum liquidus temperatures in the system Qz – Or – Ab – H_2O with added F, B_2O_3 and Li_2O from Manning et al. (1984). H_2O-saturated liquidus curve for Macusani glasses (MAC) from London et al. (1986) and Boher et al. (1987). BV and HAR: H_2O-saturated solidi of the Beauvoir granite (Boher et al. 1987; Pichavant et al. 1987b) and the Harding pegmatite (Burnham and Nekvasil 1986) respectively

conditions inferred above for the main magmatic stage (650° C, 1.5 kbar). This is another way of stating that crystallization takes place under conditions around H_2O-saturation. However, it serves to illustrate that muscovite may actually crystallize from the melt in the pressure range inferred for the main magmatic stage. The muscovite out reactions progressively shift towards higher temperatures (Fig. 17) with increasing F content in muscovite (i.e., with increasing f_{HF}/f_{H_2O} ratios, Table 10). Note that, although the calculated f_{HF} values are close to 1 bar, the f_{H_2O}/f_{HF} ratios are significantly different for the 4 muscovite compositions used in the calculations (Table 10). It is apparent, from Table 10 and Fig. 17, that the f_{H_2O}/f_{HF} ratio (hence the muscovite composition) is critically important in controlling the location of muscovite stability in granitic magmas.

The elevated f_{H_2} obtained (Table 10) reflects both low f_{O_2} (the calculations assume no H_2 loss from the early magmatic stage, see Appendix) and relatively high f_{H_2O}.

Discussion and implications for peraluminous magmas

The mineralogy of the Macusani volcanics is, in many respects (see above), similar to that of the plutonic two-mica or tourmaline leucogranites (e.g., Le Fort 1981; Price 1983; Pichavant and Manning 1984; Benard et al. 1985). Therefore, this study brings information that may help in constraining the mineralogical and magmatic evolution of felsic, strongly peraluminous magmas in general.

It is clearly shown that muscovite (Schleicher and Lippolt 1981) and andalusite (Clarke et al. 1976) may be low pressure magmatic phases in felsic peraluminous magmas. Caution is suggested when using muscovite as a petrogenetic indicator (particularly for pressure), because muscovite stability in peraluminous magmas essentially depends on 4 independent parameters: crystallization temperature, pressure, a_{H_2O} and f_{HF}. In the same way, in view of the large chemical variations found here for undoubtly magmatic muscovites, it may be difficult to use chemical discrimination diagrams (Miller et al. 1981) to infer a magmatic or postmagmatic origin for muscovite. However, the presence of phenocrystic muscovite allows the estimation of f_{H_2O} (and a_{H_2O}) during magmatic evolution, with the condition that the muscovite composition is representative of that in the magma.

The marked differences between textures, mineral assemblages, pressures and temperatures, and the abrupt variations allow to establish a clear distinction between an early magmatic stage (magmatic evolution at or near the source region), and a main magmatic stage (high level crystallization of the magmas). The implications are of considerable importance. (1) The magmas must have been generated under H_2O-undersaturated conditions; H_2O-saturation was reached relatively late in the magmatic history, in response to the combined effects of magma ascent (with subsequent pressure drop) and shallow level crystallization. This contrasts with most models on the generation of two-mica peraluminous leucogranites (e.g., Lameyre 1973; Le Fort 1973, 1981; Wickham 1987), which consider two-mica leucogranites as being generated and crystallized nearly in-situ under H_2O-saturated conditions. (2) High level crystallization (limited by the H_2O content of the melt, see above) drove magma compositions from somewhat less fractionated towards more fractionated compositions. Therefore, the chemistry of the volcanics should bear the mark of both partial melting and crystal fractionation (Pichavant et al. 1988).

Analyses of magmatic phases (e.g., muscovite, tourmaline, biotite and feldspars) are presented. In the Macusani field, a striking feature is that the chemistry of mineral phases is nearly constant. The lack of systematic variation in mineral chemistry with stratigraphic position implies parallel, but largely independent evolution of the different magma batches. This further implies no great variation in the compositions of mineral phases in the source rocks and/or in conditions of partial melting. The imprint of crystal fractionation on mineral chemistry is marked mostly by the feldspars (the rare plagioclase cores and group I plagioclases, the sanidines although their range of major element compositions is narrow), and to a minor extent by the ferromagnesian phases (a few late biotites, tourmalines, muscovites). Given the absence of large compositional variations for the early magmatic phases, crystal fractionation is considered to have been of small importance during the early magmatic history.

It has been possible to identify, mainly on the basis of textural criteria, both restites and magmatic phenocrysts among the early magmatic assemblage. This implies nearly simultaneous partial melting and crystallization in/or near the source region. Recent thermal models of crustal melting by injection of basaltic sills (Huppert and Sparks 1987) suggest that partial melting is accompanied by partial crystallization in anatectic zones subjected to high heat fluxes. This is the situation envisaged for the source region of the Macusani magmas. Heat is assumed to have been supplied

by the intrusion of hot, presumably mafic, magmas in the mid-crust (Pichavant et al. 1988). In this context, disequilibrium melting of biotite indicates local, fast elevations of temperature in the source region. The presence of early phenocrysts in the early magmatic assemblage and the low restite content of the Macusani magmas is in contradiction with the "all restite" model of Wyborn et al. (1981) and Chappell et al. (1987). By opposite, this study shows that some phenocrysts may be as early as restites. Maybe the only way to solve the "restite controversy" (Chappell et al. 1987; Wall et al. 1987) is to pay more attention to textures.

The Macusani volcanics have mineralogical features that would identify them as "S-type" magmas (e.g., White et al. 1986). However, a detailed comparison with Australian "S-type" magmas (Clemens and Wall 1981, 1984; Wyborn et al. 1981; Phillips et al. 1981; White et al. 1986) reveals differences with important petrogenetic implications (see Pichavant et al. 1988). *Firstly*, in the Macusani volcanics (and in their plutonic equivalents), the "AFM" mineralogy is characterized by biotite-muscovite, with sillimanite, andalusite, tourmaline and cordierite as typical subordinate phases. On the other hand, most of the Australian magmas have an "AFM" mineralogy dominated by biotite-cordierite assemblages. Garnet and orthopyroxene are common, but sillimanite is not systematically found and muscovite, andalusite and tourmaline are rarely mentioned. Biotite Al_2O_3 contents are significantly lower than in the Macusani volcanics. The evidence therefore points to less strongly peraluminous source rocks for the Australian "S-type magmas" than for the Macusani magmas. *Secondly*, biotite and sillimanite are the main residual phases in the Macusani magmas. Although biotite shows textures of fusion, the biotite melting was not extensive. Only a small proportion of biotite from the source rock was consumed, as indicated by the low modal abundances of cordierite-type phases and spinels. In contrast, the more mafic compositions of the Australian magmas (Pichavant et al. 1988) and their abundance in garnet, cordierite and orthopyroxene suggest that a larger proportion of biotite has reacted out in their source region. In other words, the conditions of partial melting and generation of the Macusani magmas do not largely exceed the beginning of melting of biotite-sillimanite assemblages whereas biotite stability conditions are largely overstepped during generation of the Australian magmas (see also Clemens and Wall 1981). This has important consequences concerning the control of a_{H_2O} and the origin of water for melting. Questions relative to the generation of the Macusani magmas are addressed in Part II (Pichavant et al. 1988).

Acknowledgements. Field studies, by DJK, AHC and MP have been supported since 1980 respectively by grants to AHC and E Farrar from the Natural Sciences and Engineering Research Council of Canada and by a grant from CNRS to L Briqueu (ATP Transfert 1984). Field work in Peru was carried out with the generous logistical assistance of Minsur, SA, through the good offices of Ing. F Zavalita, C L Briqueu, G Carlier and M Valencia are thanked for their help during field work in 1985. E Farrar and DJ Archibald assisted in the K – Ar dating studies. CESEV and C Esteyries are acknowledged for their participation to the early part of the laboratory work in Nancy. VE Barnes and COGEMA provided samples. JP Pupin studied the zircon typology. H Voinot and CREGU are thanked for the autoradiographies and JM Claude, A Kohler and P Ciszewski for their help with the electron microprobe and scanning electron microscope. ES Grew is acknowledged for the ion microprobe data. C Ramboz helped with the muscovite structural formulae. Special thanks to B Charoy, JM Montel and C Weber. Reviewed by C Bacon, A Brearley, J Clemens, C Miller, D Velde, E-an Zen.

Appendix: thermodynamic calculations

Pressure (early magmatic stage)

The following silica activity buffer reactions ($a^L_{SiO_2}$, Nicholls et al. 1971) have been considered:

$$\underset{\text{quartz}}{SiO_2} \rightleftharpoons \underset{\text{liquid}}{SiO_2} \quad \text{(A-1)}$$

$$\underset{\text{sillimanite}}{Al_2SiO_5} \rightleftharpoons \underset{\text{corundum}}{Al_2O_3} + \underset{\text{liquid}}{SiO_2} \quad \text{(A-2)}$$

$$0.2\ \underset{\text{garnet}}{Fe_3Al_2Si_3O_{12}} + 0.4\ \underset{\text{sillimanite}}{Al_2SiO_5} \rightleftharpoons 0.6\ \underset{\text{spinel}}{FeAl_2O_4} + \underset{\text{liquid}}{SiO_2} \quad \text{(A-3)}$$

$$0.2\ \underset{\text{cordierite}}{Fe_2Al_4Si_5O_{18}} \rightleftharpoons 0.4\ \underset{\text{spinel}}{FeAl_2O_4} + \underset{\text{liquid}}{SiO_2} \quad \text{(A-4)}$$

Reaction A-1 (quartz is absent during the early magmatic stage) and A-2 (corundum is absent) place respectively upper and lower limits on $a^L_{SiO_2}$ (standard state silica glass) during the early magmatic stage. Reactions A-3 and A-4 are equilibria between breakdown products of biotite-sillimanite assemblages (garnet, spinel and cordierite, Montel et al. 1986 b). These fix additional limits on $a^L_{SiO_2}$ since garnet is absent and spinel is present.

The calculations were carried out at 1073 K (800° C), i.e., the maximum temperature inferred for the early magmatic stage (see above). Molar volumes for quartz, SiO_2 glass, sillimanite, corundum, hercynite are taken from Robie et al. (1978) and for almandine and Fe-cordierite from Holdaway and Lee (1977). Standard state thermodynamic properties and C_p values are from Robie et al. (1978) for quartz, SiO_2 glass, corundum and from Bohlen et al. (1986) for almandine and hercynite. For sillimanite, two sets of thermodynamic data (Robie et al. 1978 and Bohlen et al. 1986) have been used. Thermodynamic data for Fe-cordierite were estimated at 1073 K from the reaction Fe-cordierite = hercynite + quartz (Holdaway and Lee 1977). The spinel composition is averaged from Table 8, Zn is treated as an inert diluent and a 3-site ideal mixing formulation is used for the activity of hercynite in spinel ($a^{Sp}_{Hc} = X^A_{Fe} \cdot X^{B2}_{Al}$, with $X^A_{Fe} = Fe^{2+}/(Fe^{2+} + Mg)$). For garnet, we chose to use an activity of 0.5 for almandine and, for cordierite, a mole fraction of 0.6 of Fe-cordierite (Vielzeuf 1983). The regions of possible values of $a^L_{SiO_2}$ during the early magmatic stage are represented as shaded areas on Fig. 18.

f_{H_2O}, f_{H_2} and f_{HF} (main magmatic stage)

The coexistence of muscovite, andalusite, sanidine and quartz buffers f_{H_2O} during the main magmatic stage according to the equilibrium:

$$\underset{\text{muscovite}}{KAl_3Si_3O_{10}(OH)_2} + \underset{\text{quartz}}{SiO_2} \rightleftharpoons \underset{\text{sanidine}}{KAlSi_3O_8} + \underset{\text{andalusite}}{Al_2SiO_5} + \underset{\text{gas}}{H_2O} \quad \text{(A-5)}$$

$$K = f_{H_2O} \cdot a^{Sa}_{Kf} / a^{WM}_{Mu}.$$

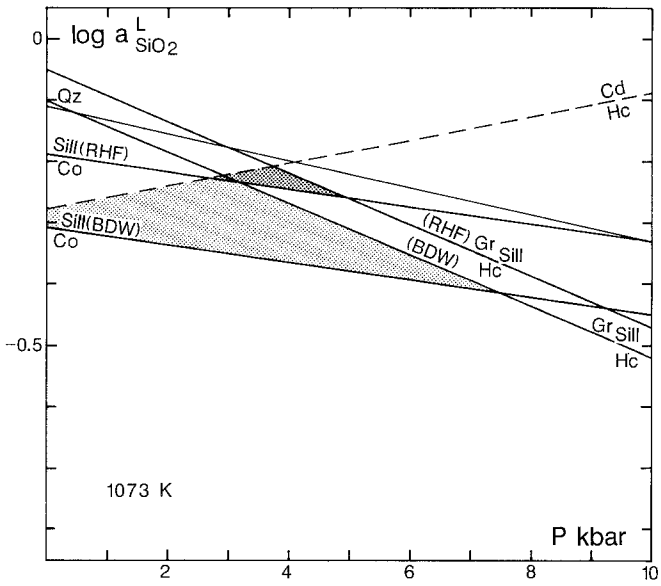

Fig. 18. Variation of $\log a^{L}_{SiO_2}$ with pressure at 1073 K (800° C) for the silica buffer reactions in the Appendix. Abbreviations as in Fig. 16 and *Gr* = garnet; *Co* = corundum. See the Appendix for details of the calculations. The two different shaded domains indicate regions of possible values of $\log a^{L}_{SiO_2}$ and *P* for the early magmatic stage. These are obtained with thermodynamic data for sillimanite from Robie et al. (1978) and Bohlen et al. (1986) respectively (abbreviated *RHF* and *BWD*). The cordierite-hercynite equilibrium is shown dashed because thermodynamic data for Fe-cordierite are imprecise (see Appendix)

a^{Sa}_{Kf} is the activity of $KAlSi_3O_8$ in sanidine and a^{WM}_{Mu} the activity of $KAl_3Si_3O_{10}(OH)_2$ in the white mica. The ΔH and ΔS of the reaction were calculated from the experimental brackets of Chatterjee and Johannes (1974). Assuming $\Delta C_p = 0$ in the temperature range of interest, the following expression is obtained for f_{H_2O} ($\log_{10}$, *P* in bars, *T* in K):

$$\log f_{H_2O} = 8.203 - 4572/T + 0.0147(P-1)/T - \log a^{Sa}_{Kf}/a^{WM}_{Mu}$$

The solid solution model of Thompson and Waldbaum (1968) was used for sanidine. It yields a value of a^{Sa}_{Kf} close to 0.9, irrespective of variations in sanidine composition (Table 4; Fig. 9). For the white micas, the activity model of Holdaway (1980) was used with an additional term for the OH−F substitution: $a^{WM}_{Mu} = X_K \cdot X^{VI2}_{Al} \cdot X^{2}_{OH}$. The hydroxyl sites are assumed to be filled, hence OH + F = 2. Calculations were made for several temperatures, $P = 1500$ and 1750 bar and for 4 muscovites from Table 5. The results for 923 K (650° C) are given on Table 10. The location, in $P_{H_2O} - T$ space, of the equilibrium A-5 for the muscovites no. 14 and 16 (F−Mu out curves, Fig. 17) was calculated for $P = 1500$ bar and using the tables of Burnham et al. (1969).

a_{H_2O} was obtained from:

$$a_{H_2O} = f_{H_2O}/f^{O}_{H_2O}$$

with $f^{O}_{H_2O}$ from Burnham et al. (1969). The H_2O content of the melt is calculated from Burnham (1979b). The melt is assumed to have a constant silicate composition, taken to be that of the ash-flow tuff MH2 (Pichavant et al. 1988). As the melt is strongly peraluminous and contains elevated B and Li (Pichavant et al. 1987a, 1988), calculated melt H_2O contents are minimum values (Burnham and Nekvasil 1986).

f_{H_2} is calculated from:

$$H_2 + 0.5\, O_2 \rightleftharpoons H_2O \qquad \text{(A-6)}$$

with log K from Robie et al. (1978) and f_{H_2O} from above. f_{O_2} was taken to be 2 log units below QFM. This assumes that f_{O_2} remained constant between the early and main magmatic stages (see above). For 923 K (650° C) and 1500 bar, $\log f_{O_2} = -20.74$ (Huebner 1971).

$\text{Log} f_{H_2O}/f_{HF}$ and f_{HF} are calculated (Table 10) from Munoz and Ludington (1977) using muscovite compositions from Table 5.

References

de Albuquerque CAR (1973) Geochemistry of biotites from granitic rocks, Central Portugal. Geochim Cosmochim Acta 37:1779–1802

Arenas MJ (1982) Memoria explicativa del mapa geologico de la Mina Santo Domingo, Puno. Report Minsur, S.A., p 9

Barnes AE, Edwards G, Mc Laughlin WA, Friedman I, Joensuu O (1970) Macusanite occurrence, age, and composition, Macusani, Peru. Bull Geol Soc Am 81:1539–1546

Benard F, Moutou P, Pichavant M (1985) Phase relations of tourmaline leucogranites and the significance of tourmaline in silicic magmas. J Geol 93:271–291

Blake S (1984) Volatile oversaturation during the eruption of silicic magma chambers as an eruption trigger. J Geophys Res 89:8237–8244

Blumel P, Schreyer WE (1977) Phase relations in pelitic and psammitic gneisses of the sillimanite-potash feldspar and cordierite-potash feldspar zones in the Moldanubicum of the Lam-Bodenmais area, Bavaria. J Petrol 18:431–459

Boher M, Stenger JF, Pichavant M (1987) Low temperature, Li-, F-rich granitic magmas. Terra Cognita 7:356

Bohlen SR, Boettcher AL, Wall VJ, Clemens JD (1983) Stability of phlogopite-quartz and sanidine-quartz: a model for melting in the lower crust. Contrib Mineral Petrol 83:270–277

Bohlen SR, Dollase WA, Wall VJ (1986) Calibration and application of spinel equilibria in the system FeO-Al_2O_3-SiO_2. J Petrol 27:1143–1156

Brearley AJ (1987a) A natural example of the disequilibrium breakdown of biotite at high temperature: TEM observations and comparison with experimental kinetic data. Mineral Mag 51:93–106

Brearley AJ (1987b) An experimental and kinetic study of the breakdown of aluminous biotite at 800° C: reaction microstructures and mineral chemistry. Bull Mineral 110:513–532

Brown M (1983) The petrogenesis of some migmatites from the Presqu'île de Rhuys, Southern Brittany, France. In: Atherton MP, Gribble CD (eds) Migmatites, melting and metamorphism. Shiva, Natwich, pp 174–200

Brown WL, Parsons I (1981) Towards a more practical two-feldspar geothermometer. Contrib Mineral Petrol 76:369–377

Burnham CW (1979a) Magmas and hydrothermal fluids. In: Barnes HL (ed) Geochemistry of Hydrothermal Ore Deposits, 2nd edn. John Wiley and Sons, New York, pp 71–136

Burnham CW (1979b) The importance of volatile constituants. In: Yoder HS Jr (ed) The evolution of the igneous rocks, Princeton University Press, Princeton, pp 439–482

Burnham CW, Nekvasil H (1986) Equilibrium properties of granite pegmatite magmas. Am Mineral 71:239–263

Burnham CW, Holloway JR, Davis NF (1969) Thermodynamic properties of water to 1000° C and 10000 bars. Geol Soc Am Spec Pap 132

Černý P, Goad BE, Hawthorne FC, Chapman R (1986) Fractionation trends of the Nb- and Ta-bearing oxide minerals in the Greer Lake pegmatitic granite and its pegmatite aureole. Am Mineral 71:501–517

Chappell BW, White AJR, Wyborn D (1987) The importance of

residual source material (restite) in granite petrogenesis. J Petrol 28:1111–1138
Charoy B (1986) The genesis of the Cornubian batholith (South-West England): the example of the Carnmenellis pluton. J Petrol 27:571–604
Chatterjee ND, Johannes W (1974) Thermal stability and standard thermodynamic properties of synthetic $2M_1$-muscovite, $KAl_3Si_3O_{10}(OH_2)$. Contrib Mineral Petrol 48:89–114
Clark AH, Palma VV, Archibald DA, Farrar E, Arenas MJ, Robertson RCR (1983) Occurrence and age of the tin mineralization in the Cordillera Oriental, southern Peru. Econ Geol 78:514–520
Clark AH, Kontak DJ, Farrar E (1984) A comparative study of the metallogenetic and geochronological relationships in the northern part of the Central Andean tin belt, SE Peru and NW Bolivia. In: Janelidze TV, Tvalchralidze AG (eds) Proceedings of the VI quadrennial IAGOD symposium. Schweizerbart'sche, Stuttgart, pp 269–279
Clark AH, Yamamura BK, Taipe Alejandro J (1987) Tungsten mineralization associated with subvolcanic pegmatite: the Palca XI deposit, Puno, southeastern Peru. GAC-MAC Ann Meet Abstracts with Programs 12:32
Clarke DB (1981) The mineralogy of peraluminous granites: a review. Can Mineral 19:3–17
Clarke DB, Mc Kenzie CB, Muecke GK, Richardson SW (1976) Magmatic andalusite from the South Mountain batholith, Nova Scotia. Contrib Mineral Petrol 56:279–287
Clemens JD, Wall VJ (1981) Origin and crystallization of some peraluminous (S-type) granitic magmas. Can Mineral 19: 111–131
Clemens JD, Wall VJ (1984) Origin and evolution of a peraluminous silicic ignimbrite suite: the Violet Town Volcanics. Contrib Mineral Petrol 88:354–371
Clemens JD, Vielzeuf D (1987) Constraints on melting and magma production in the crust. Earth Planet Sci Lett 86:287–306
Clemens JD, Holloway JR, White AJR (1986) Origin of an A-type granite: experimental constraints. Am Mineral 71:317–324
Ewart A (1963) Petrology and geochemistry of the quaternary pumice ash in the Taupo area, New Zealand. J Petrol 4:392–431
Francis GH (1959) Ignimbritas (Sillar) de la Cordillera Oriental del sur del Perù. Inst Nac. de Invest Y Foment. Minero Bol 21:13–32
French BM, Meyer HOA (1970) Andalusite and "β quartz ss" in Macusani glass, Peru. Carnegie Inst Washington Year B 68:339–342
French BM, Jezek PA, Appleman DE (1978) Virgilite: a new lithium aluminium silicate mineral from the Macusani glass, Peru. Am Mineral 63:461–465
Frost MT, Grey IE, Harrowfield IR, Mason K (1983) The dependence of alumina and silica contents on the extent of alteration of weathered ilmenites from Western Australia. Mineral Mag 47:201–208
Gil Ibarguchi JI, Martinez FJ (1982) Petrology of garnet-cordierite-sillimanite gneisses from the El Tormes thermal dome, Iberian Hercynian foldbelt (W Spain). Contrib Mineral Petrol 80:14–24
Grant JA (1985) Phase equilibria and partial melting of pelitic rocks. In: Ashworth JR (ed) Migmatites, Blackie and Sons, Glasgow, pp 86–144
Grey IE, Reid AF, Jones DG (1974) Reaction sequences in the reduction of ilmenite: 4-interpretation in terms of the Fe-Ti-O and Fe-Mn-Ti-O phase diagrams. Trans Inst Min Metall 83:C105–C111
Grey IE, Reid AF (1975) The structure of pseudorutile and its role in the natural alteration of ilmenite. Am Mineral 60:898–906
Grey IE, Li C, Watts JA (1983) Hydrothermal synthesis of goethite-rutile intergrowth structures and their relationship to pseudorutile. Am Mineral 68:981–988
Harmon RS, Barreiro BA (1984) Andean Magmatism: Chemical and Isotopic Constraints. Shiva, p 250
Harrison TM, Watson EB (1984) The behaviour of apatite during crustal anatexis: equilibrium and kinetic considerations. Geochim Cosmochim Acta 48:1467–1477
Haslam HW (1983) An isotropic alteration product of cordierite. Mineral Mag 47:238–240
Holdaway MJ (1971) Stability of andalusite and the aluminium silicate phase diagram. Am J Sci 271:97–131
Holdaway MJ (1980) Chemical formulae and activity models for biotite, muscovite, and chlorite applicable to pelitic metamorphic rocks. Am Mineral 65:711–719
Holdaway MJ, Lee SM (1977) Fe-Mg cordierite stability in high-grade pelitic rocks based on experimental, theoretical and natural observations. Contrib Mineral Petrol 63:175–198
Huebner JS (1971) Buffering techniques for hydrostatic systems at elevated pressures. In: Ulmer GC (ed) Research techniques for high pressure and high temperature. Springer, Berlin Heidelberg New York, pp 125–177
Huppert HE, Sparks RSJ (1987) The fluid dynamics of crustal melting by injection of basaltic sills. Abs Symp Origin of Granites:49
Injoque J, Miranda C, Carlier G, Sologuren W, Tijero L (1983) Evidencia de basamento pre-cambriano en la region Inchupalla-Puno. Bol Soc Geol Peru 70:25–28
James DE (1971) Plate tectonic model for the evolution of Central Andes. Bull Geol Soc Am 82:3325–3346
Joliff BL, Papike JJ, Shearer CK (1986) Tourmaline as a recorder of pegmatite evolution: Bob Ingersoll pegmatite, Black Hills, South Dakota. Am Mineral 71:472–500
Kontak DJ (1985) The Magmatic and Metallogenetic Evolution of a Craton-Orogen Interface: The Cordillera de Carabaya, Central Andes, SE Peru. PhD Thesis, Queen's Univ, p 714
Kontak DJ, Pichavant M, Clark AH (1984a) Petrology of the Pliocene peraluminous volcanics from Macusani, SE Peru. EOS 65:299
Kontak DJ, Clark AH, Farrar E (1984b) The magmatic evolution of the Cordillera Oriental of SE Peru: crustal versus mantle components. In: Harmon RS, Barrerio BA (eds) Andean Magmatism, Shiva, pp 203–219
Kontak DJ, Clark AH, Farrar E, Pearce TH, Strong DF, Baadsgaard H (1986) Petrogenesis of a Neogene shoshonite suite, Cerro Moromoroni, Puno, SE Peru. Can Mineral 24:117–135
Kontak DJ, Clark AH, Farrar E, Archibald DA (1987) Geochronological data for Tertiary granites of the southeast Peru segment of the Central Andean tin belt. Econ Geol 82:1611–1618
Korzhinskiy MA (1984) Apatite solid solutions as indicators of the fugacity of HCl^0 and HF^0 in hydrothermal fluids. Geochem Int 18:44–60
Kudo AM, Weill DF (1970) An igneous plagioclase thermometer. Contrib Mineral Petrol 25:52–65
Kulm LD, Dymond J, Dasch EJ, Hussong DM (1981) Nazca Plate: crustal formation and Andean convergence. Geol Soc Am Mem 154
Lacroix A (1893) Les enclaves des roches volcaniques. Protat Frères, p 710
Lameyre J (1973) Les marques de l'eau dans les leucogranites du Massif Central Français. Bull Soc Geol Fr 7:288–295
Laubacher G (1978) Estudio geologico de la region norte du lago Titicaca. Bol Inst Geol Mineria 5:120
Le Fort P (1973) Les leucogranites à tourmaline de l'Himalaya sur l'exemple du granite du Manaslu (Népal Central). Bull Soc Geol Fr 7:555–561
Le Fort P (1981) Manaslu leucogranite: a collision signature of the Himalaya. A model for its genesis and emplacement. J Geophys Res 86:10545–10568
Lehmann B (1978) A Precambrian core sample from the Altiplano, Bolivia. Geol Rundsch 67:270–278
Linck G (1926) Ein neuer kristallführender Tektit von Paucartambo in Peru. Chem Erde 2:157–174
London D (1984) Experimental phase equilibria in the system $LiAlSiO_4-SiO_2-H_2O$: a petrogenetic grid for lithium-rich pegmatites. Am Mineral 69:995–1004

London D, Weaver BL, Hervig RL (1986) Liquidus relations of Macusani rhyolite, an analogue for rare-element granite-pegmatite systems. GSA Abstracts with Programs 18:675

Luth WC (1976) Granitic rocks. In: Bailey DK, Mc Donald R (eds) The evolution of the crystalline rocks. Academic Press, New York, pp 335–417

Manning DAC (1981) The application of experimental studies in determining the origin of topaz-quartz-tourmaline rocks and tourmaline-quartz rock. Proc Ussher Soc 5:121–127

Manning DAC (1982) Chemical and morphological variations in tourmalines from the Hub Kapong batholith of peninsular Thailand. Mineral Mag 45:139–147

Manning DAC, Martin JS, Pichavant M, Henderson CMB (1984) The effect of F, B and Li on melt structures in the granite system: different mechanisms? NERC Rpt Progr Exp Petrol 6:36–41

Marchand J, Bossière G, Leyreloup A (1982) Pinite and pseudo-"glass" in high-grade metamorphic gneisses. A discussion of: "biotite melting in high-grade metamorphic gneisses from the Haut-Allier (French Massif Central)". Contrib Mineral Petrol 79:439–442

Maury RC, Bizouard H (1974) Melting of acid xenoliths into a basanite: an approach to the possible mechanisms of crustal contamination. Contrib Mineral Petrol 48:275–286

Mehnert KR, Büsch W (1985) The formation of K-feldspar megacrysts in granites, migmatites and augengneisses. N Jb Miner Abh 151:229–259

Miller CF, Stoddard EF, Bradfish LJ, Dollase WA (1981) Composition of plutonic muscovite: genetic implications. Can Mineral 19:25–34

Monier G, Mergoil-Daniel J, Labernardière H (1984) Générations successives de muscovites et feldspaths potassiques dans les leucogranites du massif de Millevaches (Massif Central Français). Bull Mineral 107:55–68

Monier G, Robert JL (1986a) Muscovite solid solutions in the system K_2O-MgO-FeO-Al_2O_3-SiO_2-H_2O: an experimental study at 2 kbar P_{H2O} and comparison with natural Li-free white micas. Mineral Mag 50:257–266

Monier G, Robert JL (1986b) Evolution of the miscibility gap between muscovite and biotite solid solutions with increasing lithium content; an experimental study in the system K_2O-Li_2O_2-MgO-FeO-Al_2O_3-SiO_2-H_2O-HF at 600° C, 2 kbar P_{H2O}. Comparison with natural lithium micas. Mineral Mag 50:641–651

Montel JM (1986) Experimental determination of the solubility of Ce monazite in SiO_2-Al_2O_3-K_2O-Na_2O melts at 800° C 2 kbar under H_2O-saturated conditions. Geology 14:659–662

Montel JM, Weber C, Barbey P, Pichavant M (1986a) Thermobarométrie du domaine anatectique du Velay (Massif Central, France) et conditions de genèse des granites tardi-migmatitiques. C R Acad Sci Paris 302:647–652

Montel JM, Weber C, Pichavant M (1986b) Biotite-sillimanite-spinel assemblages in high-grade metamorphic rocks: occurrences, chemographic analysis and thermobarometric interest. Bull Mineral 109:555–573

Munksgaard NC (1984) High $\delta^{18}O$ and possible pre-eruptional Rb-Sr isochrons in cordierite-bearing Neogene volcanics from SE Spain. Contrib Mineral Petrol 87:351–358

Munoz JL, Ludington SD (1974) Fluoride-hydroxyl exchange in biotite. Am J Sci 274:396–413

Munoz JL, Ludington S (1977) Fluorine-hydroxyl exchange in synthetic muscovite and its application to muscovite-biotite assemblages. Am Mineral 62:304–308

Neiva AMR (1974) Geochemistry of tourmaline (schorlite) from granites, aplites and pegmatites from Northern Portugal. Geochim Cosmochim Acta 38:1307–1317

Neiva AMR (1976) The geochemistry of biotites from granites of Northern Portugal with special reference to their tin content. Mineral Mag 40:453–466

Newell ND (1949) Geology of the Lake Titicaca region, Peru and Bolivia. Geol Soc Am Mem 36

Newell ND, Chronic J, Roberts T (1953) Upper Paleozoic of Peru. Geol Soc Am Mem 58

Nicholls J, Carmichael ISE, Stormer JC Jr (1971) Silica activity and P_{total} in igneous rocks. Contrib Mineral Petrol 33:1–20

Noble DC, Peterson PS, Vogel TA, Landis GP, Grant NK, Jezek PA (1982) Rare-element-enriched ilmenite series ash-flow tuffs containing phenocrystic muscovite, andalusite and sillimanite. Macusani region, southeastern Peru. GSA Abstracts with Programs 14:577

Noble DC, Vogel TA, Peterson PS, Landis GP, Grant NK, Jezek PA, Mc Kee EH (1984) Rare-element enriched, S-type ash-flow tuffs containing phenocrysts of muscovite, andalusite and sillimanite, southeastern Peru. Geology 12:35–39

Olesch M, Seifert F (1981) The restricted stability of osumilite under hydrous conditions in the system K_2O-MgO-Al_2O_3-SiO_2-H_2O. Contrib Mineral Petrol 76:362–367

Phillips GN, Wall VJ, Clemens JD (1981) Petrology of the Strathbogie batholith: a cordierite-bearing granite. Can Mineral 19:47–63

Pichavant M, Manning DAC (1984) Petrogenesis of tourmaline granites and topaz granites; the contribution of experimental data. Phys Earth Planet Int 35:31–50

Pichavant M, Valencia Herrera J, Boulmier S, Briqueu L, Joron JL, Juteau M, Marin L, Michard A, Sheppard SMF, Treuil M, Vernet M (1987a) The Macusani glasses, SE Peru: evidence of chemical fractionation in peraluminous magmas. In: Mysen BO (ed) Magmatic processes: physicochemical principles. Geochem Soc Special Publ 1:359–373

Pichavant M, Boher M, Stenger JF, Aissa M, Charoy B (1987b) Relations de phases des granites de Beauvoir entre 1 et 3 kbar en conditions de saturation en H_2O. Geol Fr 2–3:77–86

Pichavant M, Kontak DJ, Briqueu L, Valencia Herrera J, Clark AH (1988) The Miocene-Pliocene Macusani volcanics, SE Peru. II Geochemistry and origin of a felsic peraluminous magma. Contrib Mineral Petrol 100:325–338

Pitcher WS, Atherton MP, Cobbing EJ, Beckinsale RD (1985) Magmatism at a Plate Edge: the Peruvian Andes. Wiley, New York, p 328

Pouchou JL, Pichoir F (1984) Un nouveau modèle de calcul pour la microanalyse quantitative par spectrométrie de rayons X.I application à l'analyses d'échantillons homogènes. Rech Aerosp 3:167–192

Power GM (1968) Chemical variation in tourmaline from southwest England. Mineral Mag 36:1078–1089

Powers RE, Bohlen SR (1985) The role of synmetamorphic igneous rocks in the metamorphism and partial melting of metasediments, northwest Adirondacks. Contrib Mineral Petrol 90:401–409

Price RC (1983) Geochemistry of a peraluminous granitoid suite from north-eastern Victoria, south-eastern Australia. Geochim Cosmochim Acta 47:31–42

Robbins CS, Yoder HS (1962) Stability relations of dravite, a tourmaline. Carnegie Inst Washington Year Book 61:106–108

Robie RA, Hemingway BS, Fischer JR (1979) Thermodynamic properties of minerals and related substances at 298.15 K and 1 bar (10^5 pascals) pressure and at higher temperatures. US Geol Surv Bull 1452

Schenk K, Ambruster T (1985) Beidellite-nontronite, an alteration product of cordierite in the rhyolite from Torniella (Tuscany, Italy). N Jb Miner Mh 9:385–395

Schleicher H, Lippolt HJ (1981) Magmatic muscovite in felsitic parts of rhyolites from southwest Germany. Contrib Mineral Petrol 78:220–224

Schreyer WE, Hentschel O, Abraham K (1983) Osumilith in der Eifel und die Verwendung dieses Minerals als petrogenetischer Indikator. Tschermaks Min Petr Mitt 31:215–234

Smith JV, Brown WL (1987) Feldspar Minerals. Springer, p 828

Steiger RH, Jäger E (1977) Subcommission on geochronology: convention on the use of decay constants in geo- and cosmochronology. Earth Planet Sci Lett 36:359–362

Thompson JB Jr, Waldbaum DR (1969) Mixing properties of sani-

dine solid solutions. III Calculations based on two-phase data. Am Mineral 54:811–838
Valencia Herrera J, Pichavant M, Esteyries C (1984) Le volcanisme ignimbritique peralumineux plio-quaternaire de la région de Macusani, Pérou. CR Acad Sci Paris 298:77–82
Vielzeuf D (1983) The spinel and quartz associations in high grade xenoliths from Tallante (SE Spain) and their use in geothermometry and barometry. Contrib Mineral Petrol 82:301–311
Wall VJ, Clemens JD, Clarke DB (1987) Models for granitoid evolution and source composition. J Geol 95:731–749
Watson EB, Harrison TH (1983) Zircon saturation revisited: temperature and composition effects in a variety of crustal magma types. Earth Planet Sci Lett 64:295–304
Weber C, Pichavant M (1986) Plagioclase-liquid phase relations in the system Qz-Or-Ab-An-H_2O at 3 kbar: towards a resolution of experimental difficulties. EOS 67:408

Note added in proof

The recent two-feldspar thermometer of Fuhrmann and Lindsley (Am Mineral 73:201–215) yields concordant temperatures close to 635° C for samples JV2 and MH3 (analyses 3, 10 and 2, 4 respectively from Table 4) and confirms the range of temperature inferred for the main magmatic stage.

White AJR, Chappell BW (1977) Ultrametamorphism and granitoid genesis. Tectonophys 43:7–22
White AJR, Clemens JD, Holloway JR, Silver LT, Chappell BW, Wall VJ (1986) S-type granites and their probable absence in southwestern North America. Geology 15:115–118
Wickham SM (1987) Crustal anatexis and granite petrogenesis during low-pressure regional metamorphism: the Trois Seigneurs Massif, Pyrénées France. J Petrol 28:127–168
Wyborn D, Chappell BW, Johnston RM (1981) Three S-type volcanic suites from the Lachlan fold belt, southeast Australia. J Geophys Res 86:10335–10348
Zeck HP (1970) An erupted migmatite from Cerro de Hoyazo, SE Spain. Contrib Mineral Petrol 26:225–246

Received December 9, 1987 / Accepted July 20, 1988
Editorial responsibility: W. Schreyer